Research paper

Exploration of carboxy pyrazole derivatives: Synthesis, alkaline phosphatase, nucleotide pyrophosphatase/phosphodiesterase and nucleoside triphosphate diphosphohydrolase inhibition studies with potential anticancer profile

Pervaiz Ali Channar [a, 1], Saira Afzal [b, 1], Syeda Abida Ejaz [b], Aamer Saeed [a, *],
Fayaz Ali Larik [a], Parvez Ali Mahesar [a, c], Joanna Lecka [d, e], Jean Sévigny [d, e],
Mauricio F. Erben [f], Jamshed Iqbal [b, **]

[a] Department of Chemistry, Quaid-I-Azam University, 45320, Islamabad, Pakistan
[b] Centre for Advanced Drug Research, COMSATS University Islamabad, Abbottabad Campus, Abbottabad 22060, Pakistan
[c] Institute of Chemistry, Shah Abdul Latif University, Khairpur, 66020, Pakistan
[d] Département de microbiologie-infectiologie et d'immunologie, Faculté de Médecine, Université Laval, Québec, QC, G1V 0A6, Canada
[e] Centre de Recherche du CHU de Québec — Université Laval, Québec, QC, G1V 4G2, Canada
[f] CEQUINOR (UNLP, CONICET-CCT La Plata), Departamento de Química, Facultad de Ciencias Exactas, Universidad Nacional de La Plata, C.C. 962 (1900), La Plata, Argentina

ABSTRACT

In the present work we report the synthesis of new aryl pyrazole derivatives using 1,3-dicarbonyl motifs. The reaction was proceeded by the cyclization of pentane-2,4-dione (**1a**), 3-chloropentane-2,4-dione (**1b**) or ethyl 3-oxobutanoate (**1c**) with different aryl hydrazines. The products, which can be regarded as 1*H*-pyrazol-1-yl-one analogues (**3a-f, 3g-o, 4a-c, 5a-b**) and represent drug like molecules along with well-developed structure—activity relationships, were obtained in good to excellent yield. The structures of synthesized compounds were charcterized on the basis of FT-IR, ^{1}H NMR, ^{13}C NMR and mass spectroscopic data. Considering alkaline phosphatases (APs), nucleotide pyrophosphatases/phosphodiesterases (NPPs) and nucleoside triphosphate diphosphohydrolase as the molecular targets, the effects of these synthesized compounds were investigated on different isozymes of APs, NPPs and NTPDases. The data revealed that the synthesized compounds inhibited both enzymes but most of them inhibited tissue non-specific alkaline phosphatase (TNAP) more selectively. The antitumor activity results indicated that the synthesized derivatives have strong inhibitory effects on the growth of selected cell lines from different tissues such as breast, bone marrow and cervix (MCF-7, K-562 and Hela) but with varying intensities. Moreover the binding mode of interactions were explained on the basis of molecular docking and *in-silico* studies.

© 2018 Elsevier Masson SAS. All rights reserved.

1. Introduction

Phosphatases and kinases are the group of enzymes which play an important role in the regulation of phosphorylation and dephosphorylation reactions and help in the transfer of phosphoryl groups from one entity to another, inside as well as outside the cell [1,2]. These reactions act as a key mechanism and control many pathways of the cells including; regulation of gene expression, cell proliferation and cell differentiation activities [3,4]. They also control several metabolic processes like biosynthesis of nucleic acid building blocks and synthetase/phosphorylase pathways [5,6]. The two classes of phosphatase enzyme which are involved in the hydrolysis of phosphate-ester bonds include alkaline phosphatase (AP) and nucleotide pyrophosphatase/phospdiesterase (NPP) [7]. Alkaline phosphatase exists in two major isoforms i.e., tissue

specific alkaline phosphatase (intestinal, placental and germ-cell types) and tissue non-specific alkaline phosphatase (TNAP) [8]. They all act as membrane-bounded enzymes and are widely distributed in nature [9]. Moreover, they are also known as homodimeric enzymes having three metal ions i.e., two Zn^{+2} and one Mg^{+2}, necessary for enzymatic activity. The physiological role of alkaline phosphatases have been reported in various biological processes like cell adhesion, bone mineralization and cell signaling pathways; majorly in purinergic signaling pathways [10]. Elevated level of APs is commonly associated to the diseases of liver and bone such as obstructive jaundice, hepatitis, Paget's disease, osteomalacia, osteosarcoma, fractured bone, cirrhosis, liver tumor, liver metastasis, bone metastasis, prostatic cancer and others such as renal diseases and diabetes [11–13]. Nucleotide pyrophosphatase/phosphodiesterase (NPP), another important phosphatase, involved in the hydrolysis of phosphodiester or pyrophosphate bond in a variety of substrates such as nucleoside triphosphate, choline phosphate esters and lysophospholipids [14]. Among the seven different types (NPP1-7), only three members (NPP1-3) have been well characterized. Numerous physiological functions of NPP1-3 have been reported such as regulation of extracellular pyrophosphate levels, stimulation of cell motility, nucleotide recycling and modulation of purinergic receptor signaling [15,16]. Elevated levels of NPP1-3 is associated with bone diseases; chondrocalcinosis, diabetes and malignant cancers [17,18]. Interestingly, TNAP from alkaline phosphatase and NPP1 from nucleotide pyrophosphatase/phosphodiesterase synergize in their functions during bone mineralization process; TNAP is associated with the hydrolysis of pyrophosphate and NPP1 is associated with the regulation of extracellular pyrophosphate levels [19]. Thus the optimum level of TNAP and NPP1 is associated with the normal bone functioning and other cellular pathways [20,21]. Similarly, ecto-nucleoside triphosphate diphosphohydrolase (E-NTPDase) represent a predominant family of eukaryotic enzymes characterized by the presence of five conserved domains known as "apyrase conserved region". These domains, consisting of small stretches of amino acids containing residues, are vital for the proper functioning of enzyme. The enzyme activity also strictly depends on the presence of divalent cations such as calcium and magnesium [22]. In mammals, E-NTPDases consist of eight members and they are named as NTPDase1-8. These enzymes have varying preference for nucleotides. NTPDase 1, 3 and 8 hydrolyze nucleoside tri and diphosphate at an equal rate whereas NTPDase 2 strongly prefers nucleoside triphosphate [23].

Considering the role of TNAP and NPP1 in various pathophysiological processes along with their extracellular actions makes them an attractive target for some specific therapeutic interventions. Therefore, potent and selective inhibitors of TNAP and NPP1 might be useful candidates for the drug used in treatment or prevention of some of these diseases especially; bone mineralization dysfunctions, cancer (hepatic, breast) and its associated malignancies. A large number of compounds bearing nitrogen-containing fused heterocyclic skeletons have been reported with excellent inhibitory values and most of them also exhibited anti-cancer activity [24–28]. Encouraged by those results, aromatic heterocycles containing two nitrogen atoms in their five-membered rings have attracted considerable attention in recent studies due to their wide spectrum of biological activities as such as anticancer, analgesic, anti-inflammatory, antimicrobial, antiviral, anticonvulsant, antihistaminic and anti-HIV [29–32]. The recent success of pyrazole as COX-2 inhibitors has further highlighted the importance of these heterocycles in medicinal chemistry [33].

Pyrazole is five member cyclic compound with two adjacent nitrogen atoms. Pyrazole unit possess significance importance in synthetic chemistry, as it can be used as useful reagent in multicomponent reactions and designing of chiral catalyst [34]. Pyrazole derivatives exhibit extensive spectrum of biological activities such as anti-inflammatory, antiproliferative, anti-hepatotoxicity, antileishmanial, analgesic, anticancer, insecticidal, antimicrobial and antioxidant. Furthermore, pyrazole nucleus has been widely studied as an entry to new class of several enzyme inhibitors such as, monoamide oxidase inhibitors, BRAF (BRAF is a human gene that makes a protein called B-Raf, formally known as serine/threonine protein kinase B-Raf) inhibitors, DNA gyrase inhibitors, cyclin dependant kinase inhibitors, Interleukin receptor-associated kinase 4 (IRAK4) inhibitors, 5α-Reductase inhibitor and tissue-non-specific alkaline phosphatase (TNAP) inhibitors [35].

In recent years, several drugs have been developed from pyrazole derivatives. For example, celecoxib demonstrates anti-inflammatory effects and inhibits COX-2; rimonabant functions as a cannabinoid receptor and is utilized to treat obesity; fomepizole inhibits alcohol dehydrogenase; and sildenafil inhibits phosphodiesterase [35]. The examples of few drug molecules containing pyrazole scaffolds (Fig. 1).

Pyrazole moiety is considered as privileged unit for the designing of new enzyme inhibitors and drugs because it possess two nitrogen atoms in a five membered ring, the one nitrogen atom act as hydrogen bond donor, while the other nitrogen atom can coordinate with metal atoms. Methyl groups attached to pyrazole ring provide necessary free bond rotation (flexibility). Polarized pi ring of pyrazole sets the ground for aromatic interactions. These intriguing structural features assist to incorporate various pharmacophores to furnish potent and safe drugs. Moreover, compounds having Nitrogen as heteroatom in heterocyclic moieties display enhanced solubility and salt-formation properties that enable their oral absorption and bioavailability.

Motivated by the aforesaid bioactivities concerning the scarcity of oxygen containing pyrazole systems [36] herein, we report a mechanochemical method for synthesis of oxygen containing pyrazole derivatives. The grinding-induced method (green synthesis) not only reduces the time of reaction from several hours to a few minutes but also improves the yield compared with that of conventional conditions. Moreover, the biological data of synthesized derivatives revealed a non-selective mode of inhibition within the same group i.e., *h*-TNAP and *h*-IAP. But when the results were compared with reference to the family; APs, NPPs; except four compounds (**3g, 3h, 3j** and **4a**) rest of the compounds showed selectivity towards *h*-TNAP rather than *h*-NPP1. The anticancer assay findings may provide a support and idea to the researcher to synthesize more analogues of effective derivatives along with the exploration of more molecular pathways.

2. Results and discussion

2.1. Chemistry

The cyclocondensation of pentane-2,4-dione (**1a**) or 3-chloropentane-2,4-dione (**1b**) with different aryl hydrazides (**2a-o**) was successfully achieved in the presence of piperidine as catalyst to affords (3,5-dimethyl-1*H*-pyrazol-1-yl) (phenyl)methanone (**3a-f**) and (4-chloro-3,5-dimethyl-1*H*-pyrazol-1-yl) (phenyl) methanone derivatives (**3g-o**) respectively (Table 1 and Table 2) [37,38]. The progress of the reaction was monitored by TLC using n-hexane and ethyl acetate in the ratio of 8:2. On completion, the reaction mixture was diluted with ethyl acetate and filtered; the filtrate was concentrated and recrystallized from ethanol to afford pure products in good yield (**3a-o**).

For the second series initially, 2,4-diones 3-(phenoxy)-pentane were prepared, following a known procedure [37], by potassium carbonate mediated reaction of phenols (**2**) with 3-(chloro)
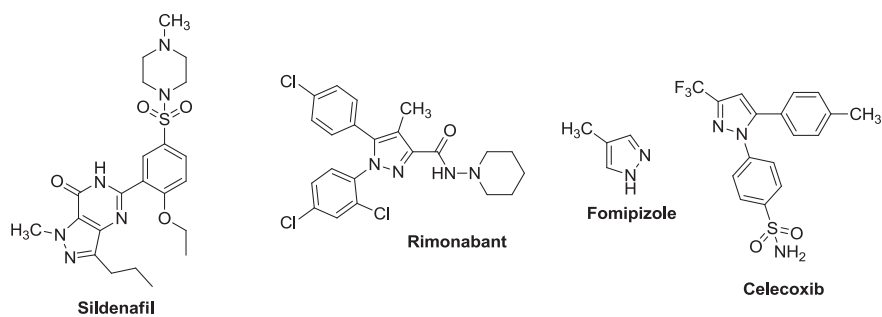
Fig. 1. Drug molecules containing pyrazole scaffolds.

Table 1
Synthesis of (3,5-dimethyl-1*H*-pyrazol-1-yl) (phenyl)methanone (**3a-f**) by grinding equimolar concentrations of pentane-2,4-dione (**1a**) with different arylhydrazides (**2a-f**).
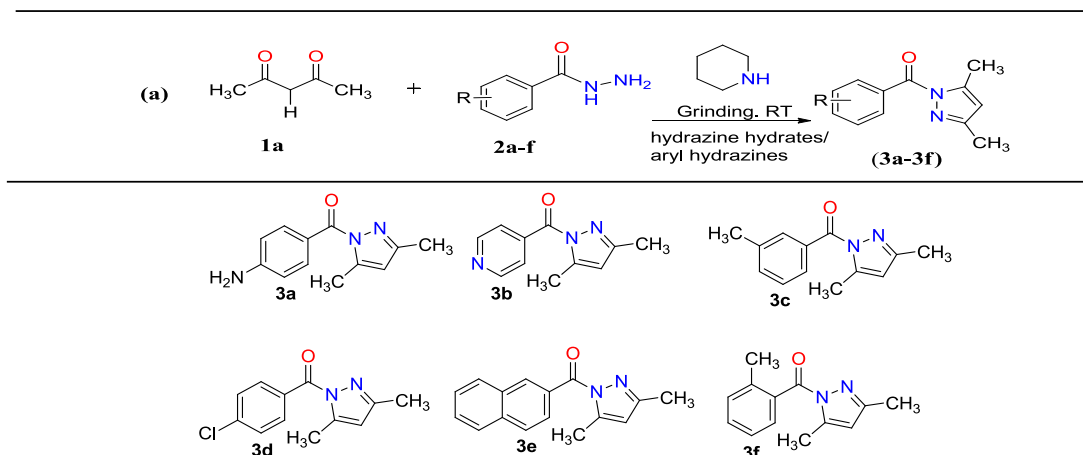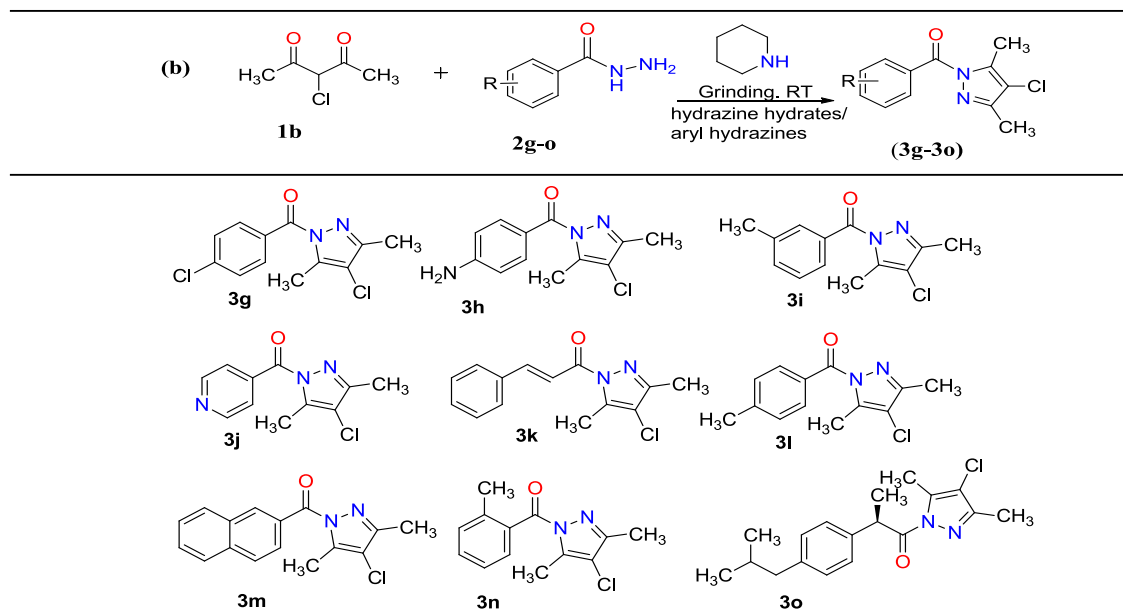

Table 2
Synthesis of (4-chloro-3,5-dimethyl-1H-pyrazol-1-yl) (phenyl)methanone (**3g-o**) by grinding 3-chloropentane-2,4-dione (**1b**) with different arylhydrazides (**2g-o**).

pentane-2,4-dione (**1b**). The corresponding 3-(phenoxy) pentane-2,4-diones which were obtained in good yield (intermediate) were further undergone cyclization reaction with different aryl hydrazides and led to the formation of 3,5-dimethyl-1*H*-pyrazol-4-ol derivatives (**4a-c**) as shown in Table 3. The reaction was carried out in the presence of piperidine under the inert atmospheric conditions. Except **4a** (70%), the % yield of the other two derivative was very low i.e., 30%.

The reaction of ethyl 3-oxobutanoate **1c** with arylhydrazide containing electron donating substituents i.e., NH_2 and CH_3 groups at position 4 of the aryl ring, was equally successful as that of the other reactions (Tables 1–3) and afforded products **5a** and **5b** in 72% yield, respectively (Table 4).

The products were characterized on the basis of their FTIR, ^{1}H NMR, mass spectroscopic and micro elemental analytical data. The stretching at 3160 (N-H), 1528 (C=N), 1597 (C=C), and 780 (C–S) cm^{-1} were noted in the FTIR spectra of pyrazoles. In ^{1}H NMR spectra, the typical sharp singlet's were noticed at δ 9.34 for NH and at δ 2.42, 2.32 ppm because of CH_3 protons". Those in the range of δ 7.31–7.83 for the aromatic protons, indicating the successful linkage of aryl through sulfur bridge. ^{13}C NMR spectra displayed the signal at δ 156.5 (C=N), 136.1 (C=C), 60.6 (C–O), and 9.6 (CH_3) ppm, in addition to those for aromatic carbons. Mechanistically, it is likely that first 3-aryloxy pentane-2,4-dione is formed as an intermediate, and then 3-aryloxy pentane-2,4-dione acetyl acetone, 3-chloro-2,4-pentanedione, compounds were then condensed with an equimolar amount of hydrazine hydrate to afford the target pyrazoles.

2.2. Biological results

2.2.1. Alkaline phosphatases (h-TNAP & h-IAP), nucleotidase pyrophosphatase/phosphodiesterase (h-NPP1 & h-NPP3) and nucleoside triphosphate diphosphohydrolase (r-NTPDase1, 2, 3 and 8) inhibition studies

All synthesized pyrazole derivatives (**3a-3o, 4a-c & 5a-b**) were tested for their potential to inhibit AP (*h*-TNAP and *h*-IAP), NPPs (*h*-NPP1 and *h*-NPP3) and nucleoside triphosphate diphosphohydrolase (*r*-NTPDase1, *r*-NTPDase2, *r*-NTPDase3 and *r*-NTPDase8) isozymes. Although these derivatives revealed a non-selective mode of inhibition within the same group i.e., APs but when the results were compared with reference to the family, except four compounds (**3g, 3h, 3j and 4a**) rest of the compounds showed selectivity towards *h*-TNAP rather than *h*-NPP1. The synthesized derivatives showed *h*-TNAP inhibition in the range of (IC$_{50}$ ± SEM) 0.91 ± 0.04 to 42.0 ± 2.62 μM, *h*-IAP inhibition in the range of (IC$_{50}$ ± SEM) 0.39 ± 0.08 to 22.3 ± 1.31 μM, *h*-NPP1 inhibition in the range of (IC$_{50}$ ± SEM) 2.53 ± 0.42 to 8.04 ± 1.01 μM and *h*-NPP3 inhibition in the range of (IC$_{50}$ ± SEM) 0.23 ± 0.05 to 5.98 ± 0.76 μM as

shown in Table 5.

The synthesized derivatives showed 20–49% inhibitory activity, when tested against rat nucleoside triphosphate diphosphohydrolase (*r*-NTPDase2, 3 and 8). However, for *r*-NTPDase1, most of the derivatives exhibited IC$_{50}$ ± SEM in lower micromolar range Table 6. For example, compound **3f**, having 2-methyl group as substituent possessed 6.21 ± 0.61 μM. Among the derivatives, (**3g-o**), **3i** showed IC$_{50}$ ± SEM = 2.30 ± 0.77 μM, while, **3n** and **3o** presented IC$_{50}$ ± SEM = 1.05 ± 1.09 and 1.10 ± 0.33 μM, respectively. Among series **4a-c**, the compound showing inhibition was **4a** with an IC$_{50}$ value of 9.02 ± 0.12 μM, and among **5a-b**, **5b** was active derivative having inhibitory concentration of 10.10 ± 0.04 μM.

2.2.2. Structure activity and structure selectivity relationship of (3,5-dimethyl-1H-pyrazol-1-yl) (phenyl)methanone derivatives (3a-3f, 3 g-3o)

In Scheme 1, total fifteen derivatives of (3,5-dimethyl-1*H*-pyrazol-1-yl) (phenyl)methanone were prepared (**3a-o**), possessing different aryl hydrazide substituents on phenyl ring (R). Briefly these fifteen derivatives were divided into two groups, the first group of six derivatives (**3a-f**) was synthesized by keeping dimethyl substituted pyrazole ring along with variably substituted R position on phenyl ring. While the second group of nine derivatives (**3g-o**) was synthesized by substituting the pyrazol ring at 3 position with electronegative atom such as chlorine atom and R position was substituted further with different groups. In this case, the possible effect of chlorine atom on the pyrazole ring and the substitutional effect (R) at phenyl ring were examined on the basis of their inhibitory effects on alkaline phosphatase (AP) isozymes and nucleotide pyrophosphatase/phosphodiesterase (NPPs) isozymes. The overall inhibitory effect of these derivatives (**3a-3f** and **3g-o**) was found to be increased on both APs and NPPs isozymes (Table 6).

It was observed that, from first group of derivatives i.e., **3a-f**, derivative **3a** revealed maximum inhibitory effects with IC$_{50}$ ± SEM = 3.58 ± 0.67 and 0.39 ± 0.08 μM on both *h*-TNAP and *h*-IAP isozymes, respectively. The detailed study of this derivative suggested that the significant inhibition might be due to the presence of strong electron donating group i.e., NH_2 at position 4 of phenyl ring. The strong electron donating group increases ~9 fold inhibitory effects on *h*-IAP isozyme as compared to *h*-TNAP. In case of other derivatives, the presence of weak electron donating group i.e., CH_3, pyridine or naphthyl ring, resulted in the reduced inhibitory effects on both enzymes as compared to **3a**. When the activity of **3c** and **3f** was compared, it was observed that substitution of CH_3 group at position 3 of phenyl ring (**3c**) resulted in higher inhibitory effects on *h*-TNAP as compared to derivative **3f** having the same CH_3 group substitution but at position 2. An inverse effect was observed by these two derivatives against *h*–IAP isozymes, derivative **3f**

Table 3
Synthesis of 3,5-dimethyl-1*H*-pyrazol-4-ol derivatives (**4a-c**) by cyclization of 3-(phenoxy)pentane-2,4-diones (**1b**) with different aryl hydrazides.
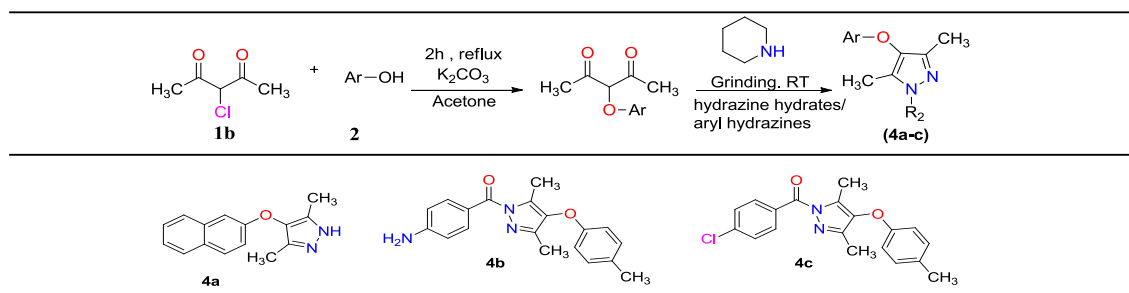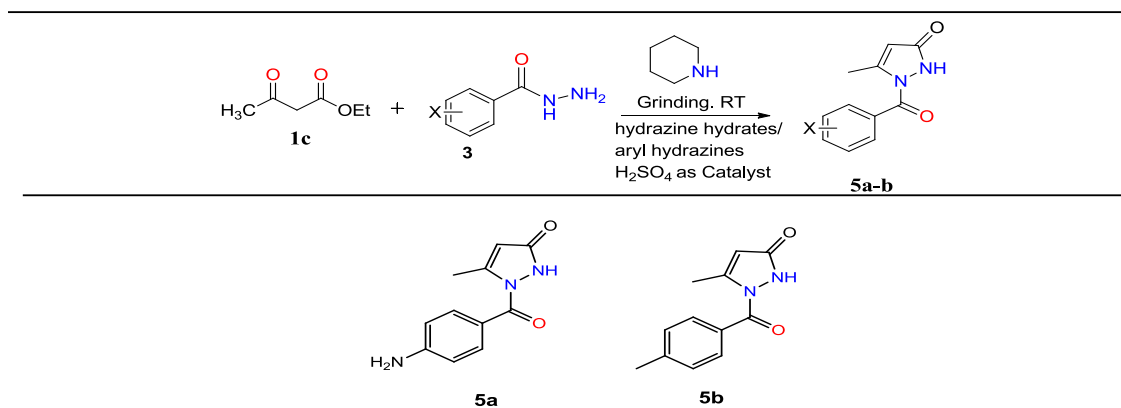
Table 4
Synthesis of 2-benzoyl-5-methyl-1*H*-pyrazol-3(2H)-one derivatives (**5a-b**) by cyclization of ethyl 3-oxobutanoate **1c** with different aryl hydrazides.

showed greater inhibition of *h*−IAP with selectivity of ~37 fold more than derivative **3c**. This showed that the stearic hindrance reduces the inhibitory behavior of these derivatives against *h*-TNAP. Other derivatives (**3d, 3e, 3b**) with weak electronegative substitution or presence of pyridine or naphthyl ring in place of phenyl ring, showed comparatively less inhibitory effects on both isozymes as compared to **3a.** Presence of pyridal group makes the molecule relatively electron deficient. Moreover, in contrast to benzene, the electron density is not evenly distributed over the ring, reflecting the negative inductive effect of the nitrogen atom. This makes compound less stable and therefore resulted in the reduced activity. Similarly, presence of bulky naphthyl group makes the compound less hydrophilic and resulted in less inhibitory effects of TNAP.

The inhibitory effect of these six derivatives on *h*-NPP1 and *h*-NPP3 isozymes was found very interesting. All of these derivatives remained inactive against *h*-NPP1 while possessed effective inhibitory activity against *h*-NPP3. Compound **3b** depicted maximum inhibition of *h*-NPP3 with $IC_{50} \pm SEM = 0.35 \pm 0.02$ μM. The structural elucidations of derivative **3b** suggested that the substitution of pyridine ring in place of substituted aryl ring possibly responsible for the enhanced inhibitory effects on *h*-NPP3. In case of compound **3e**, the attachment of napthyl ring in place of aryl ring resulted in increased inhibitory effects on *h*-NPP3 with $IC_{50} \pm SEM = 1.81 \pm 0.17$ μM but less as compared to derivative **3b**. The derivative **3d** also showed significant *h*-NPP3 inhibition with IC_{50} value of $IC_{50} \pm SEM = 1.15 \pm 0.13$ μM (Fig. 2).

The nine derivatives from the other group also influenced the activity of both enzymes to some extent depending on the type and position of substitutional functional group. The reverse effect was observed by the derivatives from both groups having similar substitution at R position but replacement of H atom with chloride group on pyrazole ring. For example the substitution of chloro group both at position 3 of pyrazol ring and position 4 (R) of phenyl ring (**3g**) resulted in enhanced inhibitory effects on *h*-TNAP, *h*-NPP1 and *h*-NPP3 as compared to derivative **3d** having no chloro group at pyrazole ring but only one chloro group at position 4 of the phenyl ring. Similarly another chloro substituted derivative **3h** possessing 4-NH2 group substitution at R position also exhibited higher inhibitory effects on NPPs isozymes in comparison to **3a** having same R substitution. The derivative **3n** exhibited the same inhibitory behavior with relation to h-NPP3 isozyme. From these results, it was observed that the substitution of chlorine atom at pyrazole ring resulted in increased inhibitory effects on NPPs.

From this group, except three derivatives i.e., **3g, 3h** and **3j**, the other six derivatives remained inactive against *h*-NPP1. The introduction of *t*-butyl group substitution at 4 position of phenyl ring (R) (**3o**) resulted in maximum inhibition of *h*-IAP as well as *h*-TNAP with the inhibitory value of $IC_{50} \pm SEM = 1.01 \pm 0.01$ and 1.07 ± 0.01 μM, respectively. Moreover, the substitution of 4-CH3 group at phenyl ring in addition to chloride substitution at pyrazole ring (**3l**) resulted in the maximum inhibitory effects on *h*-NPP3 ($IC_{50} \pm SEM = 0.23 \pm 0.05$ μM) while revealed least inhibitory effects on the other isozymes (Fig. 3).

2.2.3. Structure activity and structure selectivity relationship of 3,5 dimethyl-1H-pyrazol-4-ol derivatives

In Scheme 2, three derivatives (**4a-c**) of 3,5-dimethyl-1*H*-pyrazol-4-ol were synthesizedwith varying substitutions at position 2 and 4 on pyrazol ring. The derivative **4a** depicted least inhibitory effects on *h*-TNAP, *h*-IAP and *h*-NPP1 while it revealed significant inhibitory effects on *h*-NPP3. The structure activity relationship of derivative **4a** suggested that the substitution of naphthyl ring at R1 might be responsible for its inhibitory activity. Another derivative **4b** having substitution of *p*-tolyl group at R1 and aniline group at R2 ended up with increased inhibitory activity on *h*-TNAP and *h*-NPP3 but with abolished inhibitory effects on *h*-NPP1. Similarly another derivative (**4c**) was synthesized by keeping the same substitution at R1 like **4b** but different R2 substitution i.e., with *p*-chlorophenyl ring. The obtained results revealed that R2 position might be responsible for maximum inhibitory effects on *h*-IAP and *h*-NPP1. In both derivatives **4b** and **4c**, the substitution at R2 position determined the inhibitory effects on different isozyme. Moreover, the presence of more nucleophilic substitution at R2 position (**4b**) might be responsible for potent activity against *h*-TNAP and *h*-NPP3 (Fig. 4).

2.2.4. Structure activity and structure selectivity relationship of 2-benzoyl-5-methyl-1H-pyrazol-3(2H)-one derivatives

In Scheme 3, two more derivatives (**5a-b**) were synthesized by changing the R group on phenyl ring of 2-benzoyl-5-methyl-1*H*-pyrazol-3(2H)-one. It was observed from their structure activity relationship that the substitution of less electron donating group (4-CH3) resulted in greater inhibitory effects on *h*-TNAP and *h*-IAP while the substitution of strong electron donating group (4-NH2) resulted in significant inhibition of *h*-NPP3. Both these derivatives did not show any promising effects against *h*-NPP1.

It can be observed from the structure activity and structure selectivity relationship of **3a-o, 4a-c** and **5a-b** that in comparison to CH3 group, presence of more strong electron donating group i.e.,

Table 5
In vitro alkaline phosphatase (*h*-TNAP and *h*-IAP) and nucleotide pyrophosphatase/phosphodiesterase (*h*-NPP1 and *h*-NPP3) inhibitory activities of pyrazole derivatives 3a-o, 4a-c & 5a-b.

Code	R, R_1	*h*-TNAP	*h*-IAP	*h*-NPP1	*h*-NPP3
		IC_{50} (μM) ±SEM			
	Scheme 1 (3a-f) / (3g-o)				
3a	4-NH_2	3.58 ± 0.67	0.39 ± 0.08	>100	3.15 ± 0.18
3b	4-pyridal	6.51 ± 0.34	1.54 ± 0.12	>100	0.35 ± 0.02
3c	3-CH_3	4.58 ± 0.23	6.69 ± 0.77	>100	3.22 ± 0.17
3d	4-Cl	5.71 ± 0.16	9.81 ± 0.83	>100	1.15 ± 0.13
3e	napthyl	6.14 ± 0.56	8.07 ± 0.78	>100	1.81 ± 0.17
3f	2-CH_3	8.24 ± 0.78	0.81 ± 0.01	>100	3.42 ± 0.52
3g	4-Cl	0.91 ± 0.04	12.8 ± 1.94	5.34 ± 0.34	0.63 ± 0.04
3h	4-NH_2	7.86 ± 0.74	27.3 ± 2.11	4.35 ± 0.24	1.22 ± 0.11
3i	3-CH_3	2.59 ± 0.14	11.9 ± 1.16	>100	1.53 ± 0.06
3j	4-pyridal	42.0 ± 2.62	3.99 ± 0.32	5.42 ± 0.62	5.98 ± 0.76
3k	cinnamyl	13.3 ± 1.54	22.3 ± 1.31	>100	2.25 ± 0.31
3l	4-CH_3	17.7 ± 1.03	8.66 ± 0.95	>100	0.23 ± 0.05
3m	napthyl	19.1 ± 1.56	4.13 ± 0.56	>100	2.26 ± 0.27
3n	2-CH_3	26.4 ± 2.24	1.76 ± 0.07	>100	0.32 ± 0.02
3o	4-*t*-butyl	1.07 ± 0.01	1.01 ± 0.01	>100	12.4 ± 2.11
	Scheme 2 (4a-c)				
4a	Napthyl, H	11.12 ± 1.01	21.9 ± 1.09	8.04 ± 1.01	1.26 ± 0.07
4b	*p*-tolyl, 1-(4-amiophenyl)ethanone	4.91 ± 0.26	10.9 ± 0.93	>100	0.51 ± 0.03
4c	*p*-tolyl, 1-(4-chlorophenyl) ethanone	5.78 ± 0.23	6.26 ± 0.78	2.53 ± 0.42	2.37 ± 0.31
	Scheme 3 (5a-b)				
5a	4-NH_2	5.43 ± 0.77	15.9 ± 1.07	>100	0.41 ± 0.04
5b	4-CH_3	1.51 ± 0.06	14.1 ± 0.99	>100	1.26 ± 0.24
Levamisole		20.21 ± 1.9	–	–	–
L-Phenyl alanine		–	80.2 ± 0.001	–	–
Suramin		–	–	8.67 ± 1.3	1.27 ± 0.08

IC_{50} is the concentration at which the 50% of the enzyme activity was inhibited. All the values were expressed as IC_{50}±SEM (Standard error mean).n = 3.

NH_2 greatly enhanced the inhibitory effects of most of the derivatives on the isozymes of both selected enzyme families i.e., *h*-TNAP and *h*-IAP and *h*-NPP3 (Fig. 5).
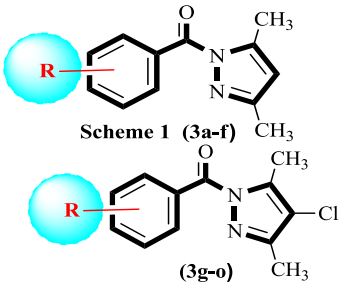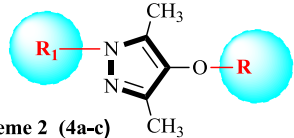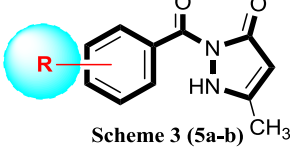
2.2.5. Molecular docking discussion

In order to identify the most possible binding interactions of the most effective derivatives within active site of target enzymes, molecular docking studies were carried out by using molecular operating environment (MOE) and LeadIT software. The most probable binding interactions of the most effective inhibitors of *h*-TNAP, *h*-IAP, *h*-NPP1 and *h*-NPP3 are shown in Figs. 5–8, respectively. The detailed 3D and 2D binding interactions of derivative **3f** within active site of *h*-TNAP is shown in Fig. 6. The amino acid residues which were involved in bonding and non-bonding interactions with **3g** included; Arg167, Ser93, Asp92, His154, His321,

His324 and His437, which played a very significant role in ligand-protein binding. Briefly, compound **3g** formed two hydrogen bonds with side chain of Ser93 and Arg167 amino acid groups. These two hydrogen bonds were formed by carbonyl group of compound **3g**. Moreover, two different π-π interactions were also formed by compound **3g** with His324 and His437. The amino acid His324 was further involved in making π-π stacked interaction with pyrazole ring while amino acid His437 was involved in forming π-π T shaped interaction with pyrazole ring in compound **3g.**

The detailed 3D and 2D binding interactions of effective inhibitor of *h*-IAP i.e., **3a** within active site of *h*-IAP is shown in Fig. 7. The amino acid residues which were involved in bonding and non-bonding interactions with **3a** included; Arg166, Ser92, Gly313, His317, Asp316, His153, His432 andAsp42 which played a very

Table 6
In vitro nucleoside triphosphate diphosphohydrolase (*r*-NTPDase1, 2, 3 and 8) inhibitory activities of pyrazole derivatives **3a-o, 4a-c** & **5a-b**.

| Code	R, R_1	r-NTPDase1	r-NTPDase2	r-NTPDase3	r-NTPDase8
		IC50 ± SEM (μM)[a]	%inhibition ±SEM[b]		

Scheme 1 (3a-f)

(3g-o)

Code	R, R_1	r-NTPDase1 IC50 ± SEM (μM)[a]	r-NTPDase2	r-NTPDase3	r-NTPDase8
3a	4-NH$_2$	37.23 ± 0.06[b]	37.89 ± 0.05	40.64 ± 0.76	41.30 ± 0.32
3b	4-pyridal	47.58 ± 0.01[b]	35.49 ± 0.12	46.79 ± 0.08	23.91 ± 0.32
3c	3-CH$_3$	41.53 ± 0.03[b]	39.81 ± 0.18	36.29 ± 0.04	33.82 ± 0.04
3d	4-Cl	36.13 ± 1.14[b]	40.77 ± 0.19	40.85 ± 0.34	25.72 ± 0.13
3e	napthyl	44.51 ± 0.89[b]	37.17 ± 0.33	43.64 ± 1.13	41.30 ± 0.55
3f	2-CH$_3$	6.21 ± 0.61[a]	43.17 ± 0.34	38.55 ± 0.05	44.93 ± 0.41
3g	4-Cl	22.36 ± 1.21[b]	30.58 ± 0.03	37.82 ± 0.11	29.95 ± 0.56
3h	4-NH$_2$	48.22 ± 0.51[b]	33.81 ± 0.15	47.27 ± 0.24	32.85 ± 0.04
3i	3-CH$_3$	2.30 ± 0.77[a]	43.53 ± 1.03	46.42 ± 1.32	46.62 ± 0.02
3j	4-pyridal	44.20 ± 0.23[b]	39.33 ± 0.10	42.91 ± 0.63	41.55 ± 1.19
3k	cinnamyl	38.51 ± 1.01[b]	34.53 ± 0.03	42.91 ± 0.59	32.61 ± 0.03
3l	4-CH$_3$	36.54 ± 0.33[b]	31.65 ± 1.03	47.63 ± 0.10	33.33 ± 0.19
3m	napthyl	44.00 ± 0.45[b]	40.53 ± 0.58	49.27 ± 1.11	44.93 ± 0.04
3n	2-CH$_3$	1.05 ± 1.09[a]	42.45 ± 0.22	37.77 ± 0.12	44.69 ± 0.35
3o	4-*t*-butyl	1.10 ± 0.33[a]	43.41 ± 0.16	48.28 ± 0.71	43.00 ± 0.14

Scheme 2 (4a-c)

Code	R, R_1	r-NTPDase1 IC50 ± SEM (μM)[a]	r-NTPDase2	r-NTPDase3	r-NTPDase8
4a	Napthyl, H	9.02 ± 0.12[a]	35.49 ± 0.21	40.24 ± 0.13	34.54 ± 0.43
4b	*p*-tolyl, 1-(4-amiophenyl)ethanone	44.68 ± 0.51[b]	38.85 ± 0.21	47.03 ± 0.66	35.51 ± 1.11
4c	*p*-tolyl, 1-(4-chlorophenyl) ethanone	58.69 ± 0.10[b]	43.88 ± 0.44	49.12 ± 0.27	49.28 ± 0.11

Scheme 3 (5a-b)

Code	R, R_1	r-NTPDase1 IC50 ± SEM (μM)[a]	r-NTPDase2	r-NTPDase3	r-NTPDase8
5a	4-NH$_2$	48.95 ± 0.12[b]	43.65 ± 0.02	38.69 ± 0.43	46.86 ± 0.89
5b	4-CH$_3$	10.10 ± 0.04[a]	45.08 ± 0.61	43.60 ± 0.22	49.28 ± 0.03
Suramin		—	—	—	—

significant role in ligand-protein binding as compared to two hydrogen bonds formed by compound **3f**, compound **3a** formed three hydrogen bonds with the side chain of Ser92, Arg166 and Gly313 amino acid residues. Among these interactions, two hydrogen bonds were formed by carbonyl group of compound **3a** with amino acid residue Ser92 and Arg166 while one hydrogen bond was formed by amine moiety with side chain of Gly313. Three different π interactions were also formed by compound **3a** with amino acid groups of His153, Arg166 and Zinc. Moreover, amino acid Arg166 was also involved in making one π-cation interaction with pyrazole ring while amino acid His153 was involved in forming one π-π T shaped interaction with benzene moiety (Fig. 7).

To check the selectivity of potent compounds against selective isozyme, the cross docking studies were carried out, i-e., potent inhibitor of *h*-TNAP (**3g**) was docked in *h*-IAP and potent inhibitor of *h*-IAP (**3a**) was docked against *h*-TNAP. The resultant results were reported in Figs. S10—S11. The Figure suggested that no strong hydrogen bond and π-π interactions were noted. However,

unfavorable (bump, red color lines) interactions were observed. It therefore suggested that which is in line with the observations in the enzyme inhibition studies and supports the high selectivity of **3a** for *h*-IAP over *h*-TNAP and **3g** for *h*-TNAP over *h*-IAP.

The detailed 3D and 2D binding interactions of the most effective inhibitor **4c** within active site of *h*-NPP1 is shown in Fig. 8. The amino acid residues which were involved in bonding and non-bonding interactions with compound **4c** included; His380. His535, Asn277, The256, Phe257, Leu290 and Lys528 which played a very significant role in ligand-protein binding. Analysis of binding interactions revealed that five different strong binding interactions were formed between compound **4c** and amino acid residue of *h*-NPP1. Among these bonding interactions, three strong hydrogen bonds were formed between compound **4c** and the side chain of Asn277, His380 and His535 amino acids. Carbonyl group was also involved in making two hydrogen bonds with amino acid residue of His380 and His53. In addition to hydrogen bonds formation, carbonyl group was also involved in making a metal interaction
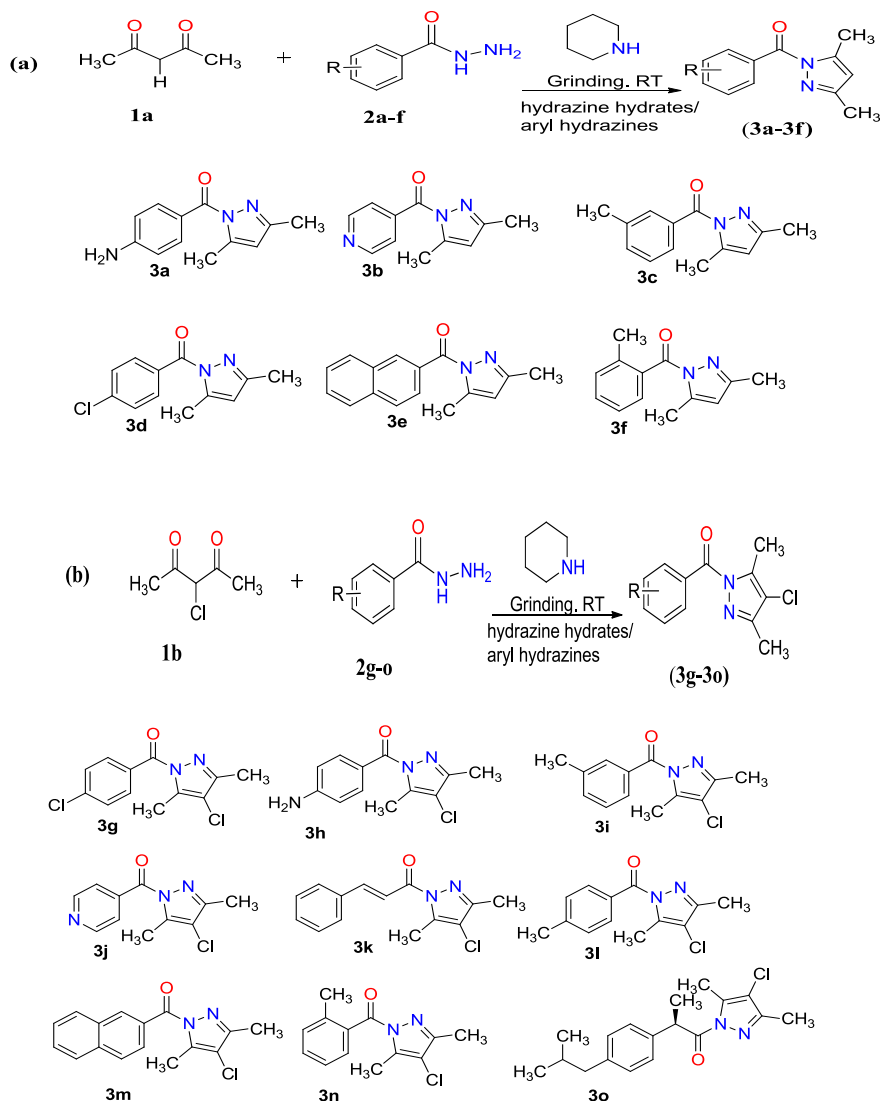
Scheme 1. A) Synthesis of (3,5-dimethyl-1*H*-pyrazol-1-yl) (phenyl)methanone (**3a-f)** by grinding equimolar concentrations of pentane-2,4-dione (**1a**) with different arylhydrazides (**2a-f**)
b)Synthesis of (4-chloro-3,5-dimethyl-1H-pyrazol-1-yl) (phenyl)methanone (**3g-o**) by grinding 3-chloropentane-2,4-dione (**1b**) with different arylhydrazides (**2g-o**).
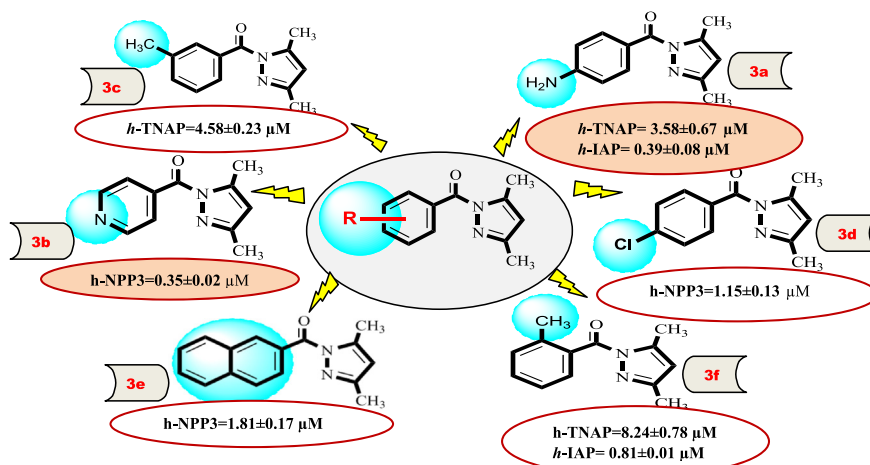

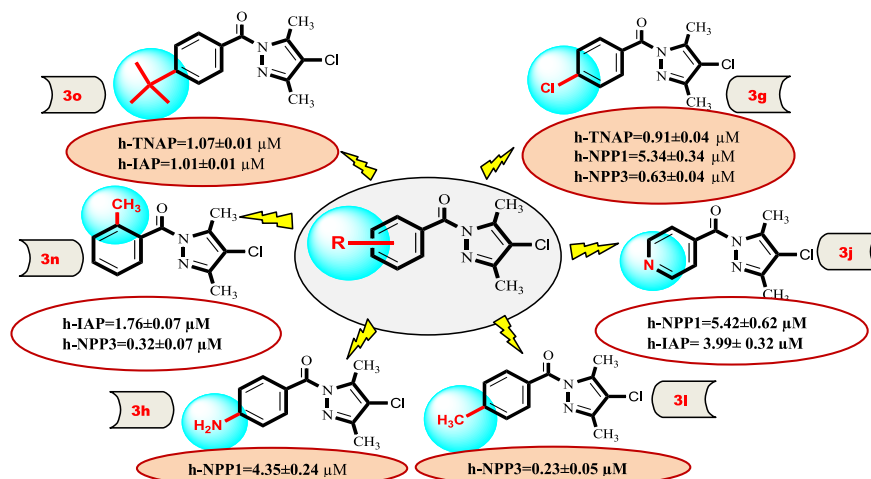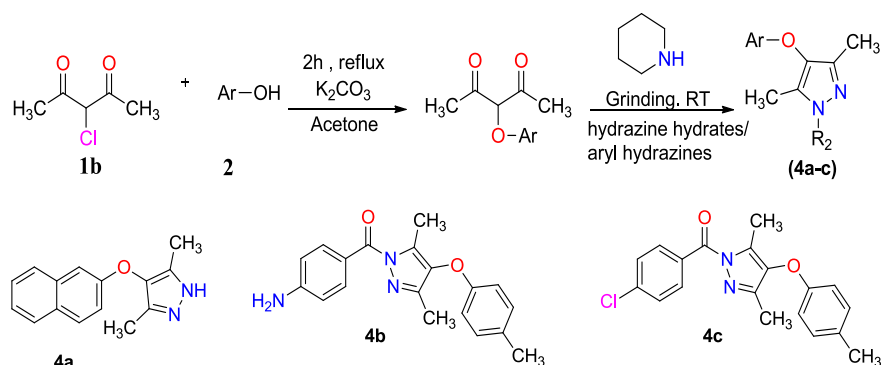**Fig. 2.** Structure-activity relationship of compounds **3a-f**.

Fig. 3. Structure-activity relationship of compounds **3g-o**.

Scheme 2. Synthesis of 3,5-dimethyl-1*H*-pyrazol-4-ol derivatives (**4a-c**) by cyclization of 3-(phenoxy)pentane-2,4-diones (**1b**) with different aryl hydrazides.
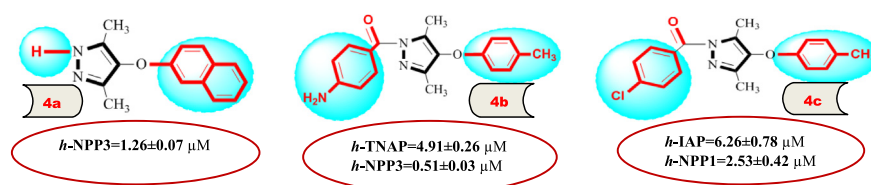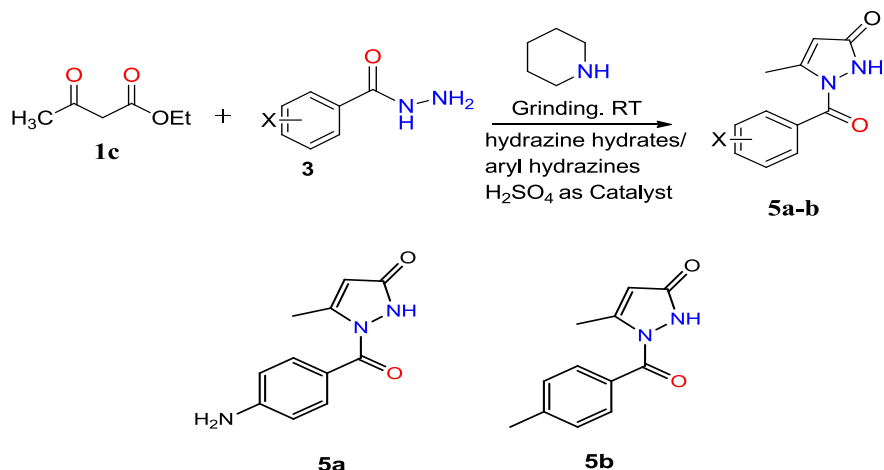

Fig. 4. Structure-activity relationship of compounds **4a-c**.

with zinc atom within the active site of *h*-NPP1. Furthermore one more hydrogen bond was also formed by nitrogen in pyrazole ring and the side chain of Asn277. Two π-π T shaped interactions were also formed by benzene ring of methylbenzene moiety and amino acid His535 as well as Tyr451 as depicted in Fig. 8.

The detailed 3D and 2D binding interactions of the most effective inhibitor of *h*-NPP3; **3l** within active site of *h*-NPP3 is shown in Fig. 9. The amino acid residues which were involved in bonding and non-bonding interactions with compound **3l** included; THr205, His483, Leu239, Tyr289, Phe206 and His329 which played a very significant role in ligand binding. Analysis of binding interactions as depicted in Fig. 9 revealed that four different strong binding interactions were formed between compound **3l** and amino acid residues of *h*-NPP3. Among these binding interactions, two strong hydrogen bonds were formed between compound **3l** and side chain of Thr205 and His483 amino acids. Carbonyl group of compound **3l** was involved in making one hydrogen bond with Thr205 and two

metal acceptor interactions with zinc atoms present within the active site of *h*-NPP3. Addition to hydrogen bond formed by carbonyl group, one hydrogen bond was also formed by nitrogen of the pyrazole ring and side chain of Asn277. Moreover, one π-π T shaped interaction was also formed by pyrazole ring and amino acid residue of His329 as shown in Fig. 9.

Similarly, the selectivity of potent compounds against selective isozymes NPP1 and NPP3 was evaluated by cross docking studies. For this purpose, the potent inhibitor of *h*-NPP1 (**4c**) was docked in *h*-NPP3 and potent inhibitor of *h*-NPP3 (**3l**) was docked against *h*-NPP1. The resultant results were reported in Figs. S12−S13. The Figure suggested that no strong hydrogen bond and π-π interactions were noted. However, many unfavorable (bump, red color lines) interactions were observed. It therefore suggested that which is in line with the observations in the enzyme inhibition studies and supports the high selectivity of **4c** for *h*-NPP1 over *h*-NPP3 and **3l** for *h*-NPP3 over *h*-NPP1.

Scheme 3. Synthesis of 2-benzoyl-5-methyl-1*H*-pyrazol-3(2H)-one derivatives (**5a-b**) by cyclization of ethyl 3-oxobutanoate **1c** with different aryl hydrazides.
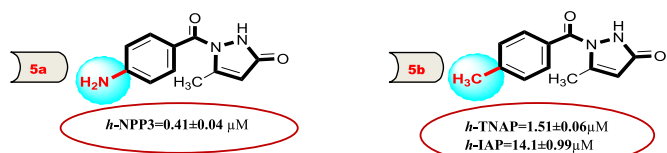

Fig. 5. Structure-activity relationship of compounds **5a-b**.

2.2.6. Cytotoxic potential by MTT assay

The synthesized pyrazole moieties i.e., **3a-o, 4a-c** and **5a-b** were subjected to *in vitro* MTT assay against cancer cell lines taken from different tissues (breast, bone marrow and cervix) in comparison to the normal cells taken from the baby hamster kidney. In order to rationalize the effect of identified inhibitors of AP and NPP iso-zymes, above mentioned cancer cell lines were selected having maximum expression of these ecto-nucleotidases [39,40]. All the synthesized derivatives were tested at the single-dose concentration of 100 μM, and the percentages of the growth reduction (inhibition) over the four tested cell lines were determined. The mean growth reduction percentages for each of the tested derivatives are illustrated in Table 7.

From Scheme 1 (**3a-f** and **3g-o**), 4-chloro substituted derivative (**3d**) exhibited stronger growth reduction of breast cancer cell line than the other derivatives of the same group containing variably substituent. Upon comparing the activities of (3,5-dimethyl-1*H*-pyrazol-1-yl) (phenyl)methanone derivatives (**3d**) and chloro substituted derivatives (at 3 position of the phenyl ring) it was observed that the substitution of chloro group both at position 3 of pyrazole ring and position 4 (R) of phenyl ring (**3g**) resulted in enhanced growth inhibitory effects on breast cancer cell line (MCF-7). These two derivatives also exhibit promising growth reduction effect on the other cell lines derived from the bone-marrow (K-562) and cervix (HeLa) but to the lesser extent than the breast cancer cells. Although the two substituted chlorine derivative exhibited much stronger effects than the derivative possessing 4-chloro phenyl substitution. From the methyl substituted derivatives, it was observed that 4-position was found more favorable for MCF-7 cells as compared to the K-562 and HeLa cell line. Among **3a-o** derivatives, the chloro substituted derivative (at pyrazole) showed stronger reduction as compared to non-chloro derivatives. The derivatives **3c** and **3i** having the electron donating methyl group at position 3 were found equi-effective, but less as compared to 4-

Fig. 6. Most Probable binding modes of the most effective inhibitor **3g** (light grey colored) within the active site of *h*-TNAP (cyan colored), Hydrogen bonds are shown in green dashed line and π-interactions are shown in pink dashed lines. 3D and 2D binding interaction are presented on left and right side respectively. (For interpretation of the references to color in this figure legend, the reader is referred to the Web version of this article.)
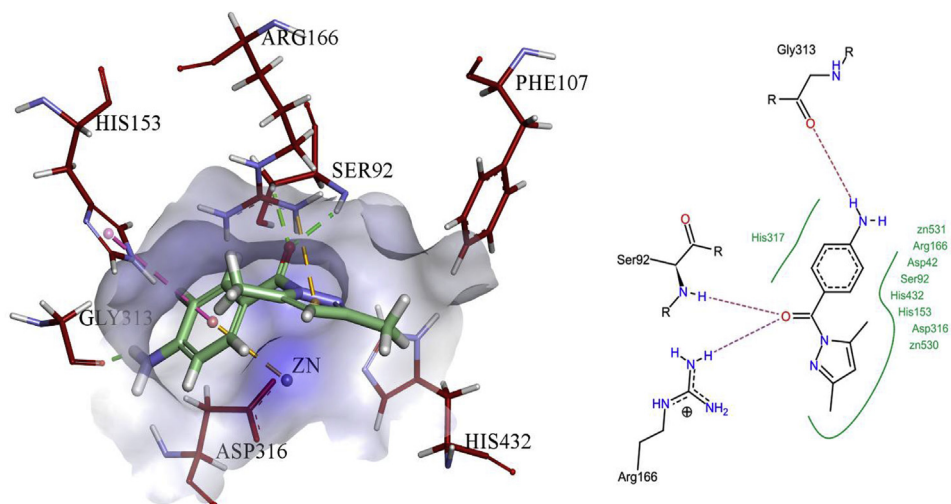
Fig. 7. Most Probable binding modes of the most effective inhibitor **3a** (light green colored) within the active site of *h*-IAP (brick colored), Hydrogen bonds are shown in green dashed line while π-interaction are shown in pink dashed lines. 3D and 2D binding interaction are presented on left and right side respectively. (For interpretation of the references to color in this figure legend, the reader is referred to the Web version of this article.)
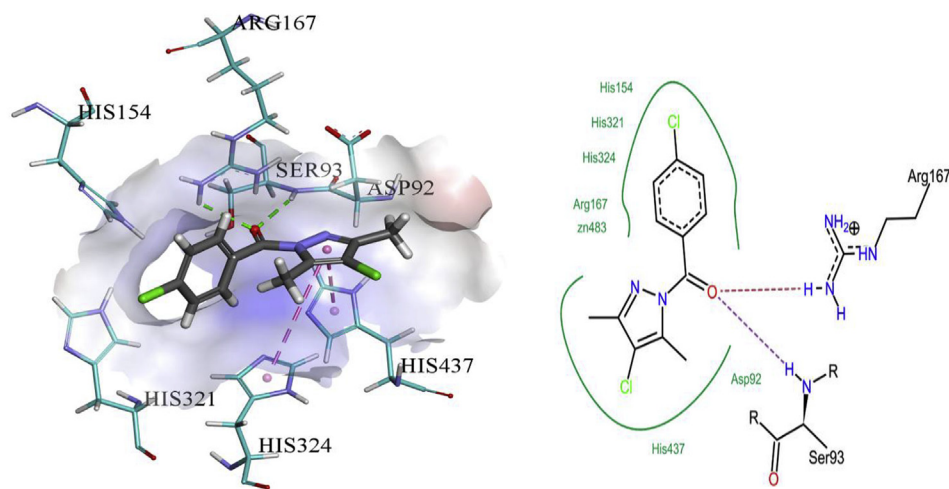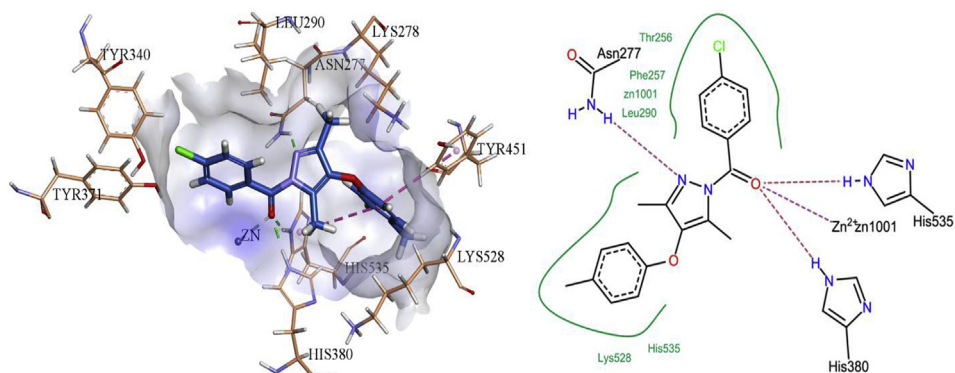

Fig. 8. Most Probable binding modes of the most effective inhibitor **4c** (light blue colored) within the active site of *h*-NPP1 (peach colored), Hydrogen bonds are shown in green dashed linewhile π-interaction are shown in pink dashed lines. 3D and 2D binding interaction are presented on left and right side respectively. (For interpretation of the references to color in this figure legend, the reader is referred to the Web version of this article.)
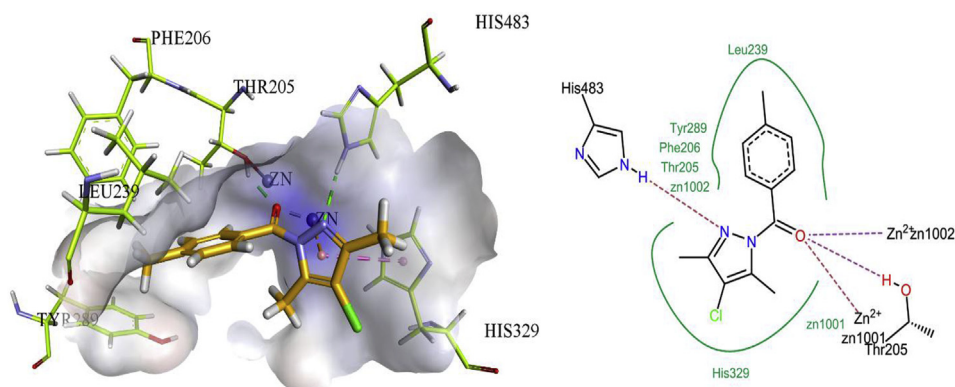
Fig. 9. Most Probable binding modes of the most effective inhibitor **3l** (gold colored) inside the active site of *h*-NPP3 (lime colored), Hydrogen bonds are shown in green dashed line while π-interaction are shown in pink dashed lines. 3D and 2D binding interaction are presented on left and right side respectively. (For interpretation of the references to color in this figure legend, the reader is referred to the Web version of this article.)

position derivatives i.e., **3l**. Moreover, the effect of 2-substituted derivatives were also observed. Compound **3f** showed higher mean growth reduction value than the corresponding derivative **3n**. Similarly from compounds **3a** and **3h** with amine substitution at 4 position, derivative **3h** was found more effective than **3a**. When the 4 position substitution was occupied with napthyl (**3e** and **3m**) and pyridal group (**3b** and **3j**) less growth reduction was observed. The reduction effect was more promising on breast cancer cell line

Table 7
Cytotoxic growth reduction effects of pyrazole derivatives (3a-o, 4a-c & 5a-b) and standard carboplatin against breast cancer cells (MCF−7), bone marrow lymphoblast cells (K−562), cervical cancer cells (HeLa) and normal/healthy baby hamster kidney cells (BHK−21) cell lines.

Code	R, R₁	-	% Growth Reduction ± SEM			
			MCF−7	K−562	HeLa	BHK−21
Scheme 1 (3a-f)						
(3g-o)						
3a	4-NH$_2$		65.2 ± 3.34	29.2 ± 2.09	58.3 ± 2.11	5.46 ± 0.17
3b	4-pyridal		68.2 ± 4.15	25.3 ± 2.11	69.7 ± 3.22	10.7 ± 1.03
3c	3-CH$_3$		67.8 ± 3.09	38.1 ± 1.77	78.4 ± 4.34	8.71 ± 0.98
3d	4-Cl		72.2 ± 4.56	64.5 ± 3.44	52.3 ± 2.77	10.3 ± 1.01
3e	napthyl		58.2 ± 1.98	67.3 ± 4.09	51.1 ± 2.88	6.53 ± 0.34
3f	2-CH$_3$		68.5 ± 2.34	60.1 ± 3.87	36.2 ± 1.87	2.78 ± 0.11
3g	4-Cl		78.7 ± 4.55	74.3 ± 4.36	72.5 ± 4.22	3.98 ± 0.32
3h	4-NH$_2$		70.3 ± 3.88	52.2 ± 2.67	63.3 ± 4.09	12.4 ± 1.09
3i	3-CH$_3$		65.9 ± 3.11	63.3 ± 4.17	75.6 ± 4.38	11.6 ± 1.06
3j	4-pyridal		63.4 ± 2.78	71.2 ± 4.88	62.9 ± 2.64	9.12 ± 0.67
3k	cinnamyl		50.1 ± 2.67	56.5 ± 3.11	72.5 ± 4.12	3.87 ± 0.32
3l	4-CH$_3$		71.2 ± 3.45	45.2 ± 3.23	68.5 ± 3.23	10.6 ± 1.01
3m	napthyl		74.7 ± 4.55	38.7 ± 2.67	66.2 ± 3.11	6.51 ± 0.45
3n	2-CH$_3$		52.6 ± 2.11	19.2 ± 1.11	71.9 ± 4.67	8.34 ± 0.71
3o	4-t-butyl		60.8 ± 2.89	47.5 ± 2.45	65.4 ± 2.89	5.11 ± 0.22
Scheme 2 (4a-c)						
4a	Napthyl, H		68.1 ± 3.45	67.8 ± 3.23	54.9 ± 2.66	5.44 ± 0.12
4b	p-tolyl, 1-(4-amiophenyl)ethanone		71.3 ± 4.11	75.1 ± 4.33	62.1 ± 2.89	6.76 ± 0.21
4c	p-tolyl, 1-(4-chlorophenyl)ethanone		54.7 ± 2.56	88.8 ± 4.89	43.9 ± 2.34	7.89 ± 0.24
Scheme 3 (5a-b)						
5a	4-NH$_2$		48.2 ± 1.99	75.4 ± 3.78	72.5 ± 3.11	12.3 ± 0.98
5b	4-CH$_3$		28.1 ± 1.23	51.1 ± 2.09	69.6 ± 2.78	14.3 ± 1.09
Carboplatin			90.7 ± 3.47	82.8 ± 2.83	85.2 ± 2.23	14.5 ± 1.01

(MCF-7) than that of the cells obtained from bone-marrow i.e., (K-562). When the obtained mean growth inhibition values were compared with the results obtained during the enzyme inhibition assay, it was interestingly observed that derivatives from both groups of Scheme 1 having substitution at position 4 of the phenyl ring, exhibited stronger enzyme inhibition effects as well as maximum growth reduction effects on cancer cell lines. It can be concluded from the enzyme inhibition data as well as anticancer potential, that the activity 4-position substituted derivatives was because of the presence of electron-withdrawing groups such as chloro.

Similarly from 3,5 dimethyl-1H-pyrazol-4-ol (4a-c) derivatives, the chloro substituted derivative (4c) exhibited stronger growth inhibition effects than the other two derivatives. The growth inhibitory effects 4c were found more on K-562 cell line along with the moderate inhibitory effects on the other selected cell lines. Moreover, amine substituted derivative (4b) showed higher inhibition than the naphthyl substituted derivative (4a), but less in comparison to the chloro substituted derivative (4c). Both derivatives of 2-benzoyl-5-methyl-1H-pyrazol-3(2H)-one (5a-b) showed more promising growth reduction effects on K-562 and HeLa cells as compared to MCF-7 cells. Here, amino substituted derivatives showed much growth reduction than the methyl substituted derivative.

2.2.7. Drug likeness evaluation and ADME properties

Now-a-days, evaluation of ADME-Tox (Adsorption, Distribution, Metabolism, and Excretion) properties and drug likeliness

Table 8
In silico ADME evaluation of synthetic compounds 3a-o, 4a-c & 5a-b.

Codes	MWt	logD	logP	logSw	HBD	HBA	TPSA	Oral Bioavailability
3a	215.256	1.933	1.965	1.933	2	4	60.91	Good
3b	201.229	1.223	1.416	1.223	0	4	47.78	Good
3c	214.269	2.491	2.776	2.491	0	3	34.89	Good
3d	234.687	2.855	3.044	2.855	0	3	34.89	Good
3e	250.302	3.344	3.312	3.344	0	3	34.89	Good
3f	214.26	2.440	2.776	2.440	0	3	34.89	Good
3g	269.132	3.428	3.576	3.428	0	3	34.89	Good
3h	249.701	2.191	2.098	2.191	2	4	60.91	Good
3i	250.73	2.827	2.448	2.827	0	3	34.89	Good
3j	235.674	1.806	1.965	1.806	0	4	47.78	Good
3k	260.725	3.223	3.216	3.223	0	3	34.89	Good
3l	248.714	3.184	3.308	3.184	0	3	34.89	Good
3m	284.747	3.993	3.824	3.993	0	3	34.89	Good
3n	248.714	3.005	3.308	3.005	0	3	34.89	Good
3o	318.849	4.885	4.258	4.885	0	3	34.89	Good
4a	238.291	3.915	2.733	3.915	1	3	37.91	Good
4b	321.381	3.747	2.966	3.747	2	5	70.14	Good
4c	340.812	4.984	3.981	4.984	0	4	44.12	Good
5a	217.229	0.161	1.49	0.624	3	5	80.88	Good
5b	216.241	0.488	2.291	1.521	1	4	54.86	Good

properties of the synthesized compounds has become an important factor for the designing of new drugs. The initial findings of ADME properties can help to cut down the total R&D cost by screening out the unwanted molecules in the initial stages of drug discovery process. For the estimation of drug likeness properties of compounds, physicochemical parameters were calculated using Med-Chem Designer [39]. The calculated ADME-Tox parameters of compounds **3a-o, 4a-c & 5a-b** are given in Table- 8. The logP value (octanol-water partition coefficient) serves as a measure of lipophilicity. Preferably the logP value should not be greater than five and it can be seen from Table- 8 that all the derivatives had logP values in the range 1.49–4.258. LogD (pH dependent octanol-water partition coefficient) was also calculated for all the derivatives and it was observed that all the compounds had favorable logD values in the range 0.161–4.984. Moreover, logSw (Logarithm of water solubility) of compound was also calculated and values for compounds **3a-o, 4a-c & 5a-b** were in the range 0.624–4.984. Furthermore, the most important aspect of these derivatives i.e., topological Polar Surface Area (TPSA) values give an estimation of surface contributions of polar moieties of the compounds. It is also useful for the determination of the ability of molecules to cross the blood brain barrier (BBB). The values are given in Table 8. Most of the obtained values were <40, indicating it's potential to reach the brain quickly, bypassing the BBA cut off filter <60. According to Lipinski's rule of 5, total number of hydrogen bond donors (HBD) should not be more than 5, and total number of hydrogen bond acceptors (HBA) should not be greater than 10. Except few derivative i.e., **3a, 3h, 4a, 4b, 5a & 5b,** rest of the derivatives did not contain any hydrogen bond donar moieties. The number of hydrogen bond acceptors was less than 5 for all the derivatives. It was observed from the computed values that all the compounds have <500 molecular weight, <5 HBD number, <10 HBA number and also <5 logP values. Therefore these derivatives can be considered to have good oral-bioavailability as well as ADME profile [40].

3. Conclusion

It was concluded from the above discussion that the inhibitory effects of synthesized pyrazole moieties were found dependent on both type and position of the functional group. Moreover, these derivatives were found least effective against *h*-NPP1 and in comparison to *h*-NPP1, except **3g, 3h, 3j, 4a** and **4c**, we got rest of the

derivatives as selective inhibitors of *h*-TNAP with effective inhibitory values. These derivatives might be useful for the exploration of their mechanism of inhibition at the molecular level where the lead molecules are required for the treatment of health disorders associated with the over-expression of *h*-TNAP. From the anticancer profile, it can be concluded that from Scheme 1, compounds **3g** and **3d** having electronegative substitution were found more effective against *h*-TNAP as well as on the breast cancer cell line. Similarly, the compounds having 4-substituted methyl group (**3l**) were found less effective on the selected targets also showed less response on the selected cell lines. The chloro derivative from Scheme 2 was found most effective against *h*-NPP1 as well as on cancer cells. Moreover, the derivative from Scheme 3 showed moderate effects but strong electron donating group showed higher inhibitory effects than the less strong electron donating methyl group.

4. Experimental

4.1. Chemistry

Melting points were recorded using a digital Gallenkamp (SANYO, Moriguchi, Japan) model MPD BM 3.5 apparatus and were uncorrected. ^{1}H NMR spectra were determined as $CDCl_3$ solutions at 300 MHz using a Bruker AM-300 spectrophotometer (Billerica, MA, USA). FTIR spectra were recorded using Bio-Rad Excalibur FTS 3000 MX spectrophotometer (Madison, WI), Mass Spectra (EI, 70 eV) on a GC-MS instrument. The reactions were carried out in glass mortar and pestle.

4.1.1. General procedure for the preparation of (substituted phenyl) (3,5-dimethyl-1H-pyrazol-1-yl) methanone derivatives (3a-3o), (4a-c) and (5a-b)

A mixture containing acetyl acetone, 3-chloro-2,4-pentanedione, 3-aryloxy-2,4-pentanediones and ethyl acetoacetate was ground in the presence of piperidine as a catalyst. The reaction was carried out in a glass mortar and pestle at room temperature. After grinding for 5–10 min, hydrazine hydrate or suitable aryl hydrazines (1 mmol) was added, and the grinding was continued for further 10 min. The progress of the reaction was monitored by TLC using *n*-hexane/ethyl acetate (8:2). On completion, the reaction mixture was diluted with ethyl acetate and filtered to remove salts, and the filtrate was concentrated.

Recrystallization from ethanol afforded pure products (**3a**–**3o**), (**4a-c**) [38] and (**5a-b**).

4.1.1.1. (4-Aminophenyl) (3,5-dimethyl-1H-pyrazol-1-yl)methanone (3a). Orange Solid (710 mg, 71%), m. p; 147–151 °C, R_f; 0.42 (Pet Ether: Ethyl Acetate; 8:2), **¹H NMR;** (300 MHz, CDCl$_3$): δ = 7.95 (d, 2H, J = 8.0 Hz, ArH), 6.68 (d, 2H, J = 7.5 Hz, ArH), 6.042 (s, 1H, CH), 2.6 (s, 3H, CH$_3$), 2.28 (s, 3H, CH$_3$), 4.10 (s, 2H, NH$_2$); **¹³C NMR;** (75 MHz, CDCl$_3$): δ = 167.5 (C=O), 151.2 (Ar-C), 151.0 (Ar-C), 144.7 (Ar-C), 134.3 (Ar-C), 122.0 (Ar-C), 113.4 (pyrazole-C), 110.3 (pyrazole-C) 14.1 (CH$_3$), 13.9 (CH$_3$). **IR;** (KBr, cm^{-1}): 3437(NH); 3131 (sp^{2}CH), 2923 (sp^{3}CH), 1661(C=O), 1513 (C=N), 1597-1479 (C=C), **GC-MS;** (EI, 70 eV): m/z (%): 216 M + 1, 215(10), 136(12), 120 (100), 95 (8), 92 (60), 82 (51); Elemental Analysis: calculated C, 66.96; H, 6.09; N, 19.52; Found C, 66.93; H, 6.07; N, 19.50; accurate mass 215.1.

4.1.1.2. (3,5-Dimethyl-1H-pyrazol-1-yl) (pyridin-4-yl)methanone (3b). Light brown (750 mg, 75%), m. p; 237–240 °C, R_f; 0.45 (Pet Ether: Ethyl Acetate; 8:2), **¹H NMR;** (300 MHz, CDCl$_3$): δ = 7.79–8.79 (m, 4H, pyridine), 5.80 (s, 1H, CH), 2.35 (s, 3H, CH$_3$), 2.10 (s, 3H, CH$_3$), **¹³C NMR;** (75 MHz, CDCl$_3$): δ = δ 166.7 (C=O), 151.4 (Pyr-C), 151.4 (Pyr-C), 149.5 (Pyr-C), 140.5 (Pyr-C), 138.7 (Pyr-C), 124.7 (Pyr-C), 124.7 (Pyrazole-C), 113.4 (Pyrazole-C), 13.8 (CH$_3$), 12.7 (CH$_3$). **IR;** (KBr, cm^{-1}): 3200 (sp^{2}CH), 2954 (sp^{3}CH), 1730 (C=O), 1561 (C=N), 1580-1476 (C=C), **GC-MS;** (EI, 70 eV): m/z (%):202 M + 1; 201 (12), 122 (13), 106 (100), 95 (8), 82 (51); Elemental Analysis: calculated; C, 65.66; H, 5.51; N, 20.88; Found C, 65.64; H, 5.54; N, 20.83, accurate mass: 201.2.

4.1.1.3. (3,5-Dimethyl-1H-pyrazol-1-yl) (m-tolyl)methanone (3c). Yellow Oil (84%), R_f; 0.60 (Pet Ether: Ethyl Acetate; 8:2), **¹H NMR;** (300 MHz, CDCl$_3$): δ = 7.72 (s, 1H, N-H), 7.68–7.54 (m, 1H, Ar-H), 7.42–7.30 (m, 2H, Ar-H), 6.09 (s, 1H, CH), 2.5 (s, 3H, CH$_3$), 2.35 (s, 3H,CH$_3$), 2.30 (s, 3H, CH$_3$), **¹³C NMR;** (75 MHz, CDCl$_3$); δ = δ 166.1 (C=O), 149.8 (Ar-C), 140.1 (Ar-C), 138.8 (Ar-C), 134.1 (Ar-C), 131.8 (Ar-C), 129.5 (Ar-C), 129.1 (Ar-C), 127.9 (pyrazol-C), 113.4 (pyrazole-C), 21.2 (CH$_3$), 13.1 (CH$_3$), 12.2 (CH$_3$). **IR;** (KBr, cm^{-1}): 3135 (sp^{2}CH), 2955 (sp^{3}CH), 1668 (C=O), 1540 (C=N), 1598-1480 (C=C); **GC-MS;** (EI, 70 eV); m/z (%): 215 M + 1; 214 (13), 135 (16), 119 (100), 95 (11), 91 (68), 82 (57); Elemental Analysis: calculated; C, 72.87; H, 6.59; N, 13.07; Found; C, 72.85; H, 6.53; N, 13.04 accurate mass: 214.1.

4.1.1.4. (4-Chlorophenyl) (3,5-dimethyl-1H-pyrazol-1-yl)methanone (3d). Light yellow solid (800 mg, 80%), m. p; 138 °C, R_f; 0.71 (Pet Ether: Ethyl Acetate; 8:2), **¹H NMR;** (300 MHz, CDCl$_3$): δ = 7.73 (d, 2H, J = 7.8 Hz, ArH), 7.47 (d, 2H, J = 7.8 Hz, ArH), 6.07 (s, 1H, CH), 2.5 (s, 3H, CH$_3$), 2.27 (s, 3H, CH$_3$); **¹³C NMR;** (75 MHz, CDCl$_3$); δ = 166.7 (C=O), 148.5 (Ar-C), 138.7 (Ar-C), 138.7 (Ar-C), 132.8 (Ar-C), 129.8 (Ar-C), 129.8 (Ar-C), 129.2 (Ar-C), 129.2 (Pyrazole-C), 113.4 (Pyrazole-C), 12.7 (CH$_3$), 12.3 (CH$_3$). **IR;** (KBr, cm^{-1}): 3110 (sp^{2}CH), 2962 (sp^{3}CH), 1700 (C=O), 1600-1559 (C=C); 1490 (C=N), **GC-MS;** (EI, 70 eV); m/z (%): 235 M + 1; 234 (M$^+$,^{37}Cl, 24), 232 (M$^+$,^{35}Cl, 74),135(12), 139.5 (100), 95 (8), 112 (60), 82(51); Elemental Analysis: Calculated; C, 61.41; H, 4.72; Cl, 15.11; N, 11.94; Found C, 61.39; H, 4.69; N, 11.90, accurate mass 234.2.

4.1.1.5. (3,5-Dimethyl-1H-pyrazol-1-yl) (naphthalen-2-yl)methanone (3e). Light brown (650 mg, 65%), m. p; 215 °C, R_f; 0.63 (Pet Ether: Ethyl Acetate; 8:2), **¹HNMR;** (300 MHz, CDCl$_3$): δ = 9.08 (m, 1H, N-H), 9.08–7.59 (m, 4H, Ar-H), 8.19 (d, J = 7.5 Hz, 1H, Ar-H) 7.51 (d, J 7.5, 1H, Ar-H), 6.22 (s, 1H, CH), 2.5 (s, 3H, CH$_3$), 2.4 (s, 3H, CH$_3$). **¹³C NMR;** (75 MHz, CDCl$_3$); δ 166.0 (C=O), 150.5 (Ar-C), 139.7 (Ar-C), 137.0 (Ar-C), 134.5 (Ar-C), 134.0 (Ar-C), 130.3 (Ar-C), 129.7 (Ar-C), 128.7 (Ar-C), 128.2 (Ar-C), 127.0 (Ar-C), 126.5 (Ar-C), 125.5 (Pyrazole-C), 113.4 (Pyrazole-C), 12.8 (CH$_3$), 11.3 (CH$_3$); **IR;** (KBr, cm^{-1}): 3140(sp^{2}CH), 2980(sp^{3}CH), 1681 (C=O),1605-1550 (C=C); 1510(C=N), **GC-MS;** (EI, 70 eV): m/z (%):251 M + 1; 250 (14), 171 (12), 155 (100), 95 (9); Elemental Analysis: Calculated; C, 76.78; H, 5.64; N, 11.19; Found; C, 76.75; H, 5.61; N, 11.15 accurate mass: 250.1.

4.1.1.6. (3,5-dimethyl-1H-pyrazol-1-yl) (o-tolyl)methanone (3f). Yellow Oil (84%), R_f; 0.60 (Pet Ether: Ethyl Acetate; 8:2), **¹H NMR;** (300 MHz, CDCl$_3$): δ = 7.68–7.32 (m, 4H, Ar-H), 6.09 (s, 1H, CH), 2.51 (s, 3H, CH$_3$), 2.45 (s, 3H, CH$_3$), (CH$_3$), 2.60 (s, 3H, CH$_3$), **¹³C NMR;** (75 MHz, CDCl$_3$): δ = δ 167.1 (C=O), 148.8 (Ar-C), 142.1 (Ar-C), 139.8 (Ar-C), 135.1 (Ar-C), 131.7 (Ar-C), 129.6 (Ar-C), 129.3 (Ar-C), 126.9 (Pyrazole-C), 114.5 (pyrazole-C), 21.3 (CH$_3$), 13.2 (CH$_3$), 12.7 (CH$_3$). **IR;** (KBr, cm^{-1}): 3134 (sp^{2}CH), 2956 (sp^{3}CH), 1666 (C=O), 1542 (C=N), 1598-1482 (C=C); **GC-MS;** (EI, 70 eV): m/z (%):215 M + 1; 212 (13), 136 (16), 118 (100), 98 (11), 95 (68), 82 (57); Elemental Analysis: Calculated; C, 72.87; H, 6.59; N, 13.07, Found; C, 72.84; H, 6.55; N, 13.04 accurate mass: 214.2.

4.1.1.7. (4-Chloro-3,5-dimethyl-1H-pyrazol-1-yl) (4-chlorophenyl) methanone (3g). White Solid (600 mg, 60%), m. p, 155 °C, R_f; 0.55 (Pet Ether: Ethyl Acetate; 8:2), **¹H NMR;** (300 MHz, CDCl$_3$): δ = 7.90 (d, 2H, J = 7.5 Hz, ArH), 7.42 (d, 2H, J = 7.5 Hz, ArH), 2.6 (s, 3H, CH$_3$), 2.24 (s, 3H, CH$_3$), **¹³C NMR;** (75 MHz, CDCl$_3$): δ = 166.3 (C=O), 152.4 (Ar-C), 139.7 (Ar-C), 134.0 (Ar-C), 132.8 (Ar-C), 129.8 (Ar-C), 129.8 (Ar-C), 129.2 (Ar-C), 129.2 (Ar-C), 119.4 (Pyrazole-C), 11.7 (Pyrazole-C), 9.8 (CH$_3$). **IR;** (KBr, cm^{-1}): 3100 (sp^{2}CH), 2972 (sp^{3}CH), 1700 (C=O), 1582 (C=N), 1590-1487 (C=C), 614–732 (C-Cl) **GC-MS;** (EI, 70 eV): m/z (%):270 M + 2, 269 M + 1; 269 ([M]+, [2 × ^{37}Cl], 3), 266 ([M]+, [^{37}Cl],[^{35}Cl], 15), 156 ([M]+, [2 × ^{35}Cl], 23), 140 (100), 130 (8), 112 (60), 82 (51); Elemental Analysis: calculated; C, 53.55; H, 3.75; N, 10.41; Found C, 53.52; H, 3.71; N, 10.39 accurate mass: 268.1.

4.1.1.8. (4-aminophenyl) (4-chloro-3,5-dimethyl-1H-pyrazol-1-yl) methanone (3h). Orange Solid (600 mg, 60%), m. p; 149 °C, R_f; 0.41, (Pet Ether: Ethyl Acetate; 8:2), **¹H NMR;** (300 MHz, CDCl$_3$):δ = 7.55 (d, 2H, J = 7.5 Hz, ArH), 6.73 (d, 2H, J = 7.5 Hz, ArH), 4.14 (s, 2H, NH$_2$), 2.6 (s, 3H, CH$_3$), 2.31 (s, 3H, CH$_3$), **¹³C NMR;** (75 MHz, CDCl$_3$): δ = 166.3 (C=O), 152.7 (Ar-C), 150.4 (Ar-C), 134.0 (Ar-C), 131.8 (Ar-C), 131.8 (Ar-C), 122.8 (Ar-C), 119.4 (Ar-C), 112.3 (Pyrazole-C), 112.3 (Pyrazole-C), 12.7 (CH$_3$), 10.9 (CH$_3$). **IR;** (KBr, cm^{-1}): 3147 (sp^{2}CH), 2933 (sp^{3}CH), 1673 (C=O), 1560 (C=N), 1597-1489(C=C), 695-570(C-Cl); **GC-MS;** (EI, 70 eV): m/z (%):251 M + 2, 250 M + 1; 249 (M$^+$, ^{37}Cl, 17), 247 (M$^+$, ^{35}Cl, 62), 136(12), 130 (8), 120 (100), 92 (60), 82 (51); Elemental Analysis: calculated, C, 57.72; H, 4.84; N, 16.83; Found C, 57.70; H, 4.80; N, 16.80; accurate mass: 249.1.

4.1.1.9. (4 -Chloro-3,5-dimethyl-1H-pyrazol-1-yl) (m-tolyl)methanone (3i). Yellow Oil (62%), R_f; 0.47 (Pet Ether: Ethyl Acetate; 8:2), **¹H NMR;** (300 MHz, CDCl$_3$): δ = 7.70 (d, J = 1.2 Hz, 1H, Ar-H), 7.68–7.54 (m, 1H, Ar-H), 7.42–7.30 (m, 2H, Ar-H), 2.50 (s, 3H, CH$_3$), 2.36 (s, 3H, CH$_3$), 2.29 (s, 3H, CH$_3$); **¹³C NMR;** (75 MHz, CDCl$_3$): δ = 165.6 (C=O), 150.4 (Ar-C), 140.1 (Ar-C), 134.0 (Ar-C), 133.1 (Ar-C), 131.8 (Ar-C), 129.5 (Ar-C), 129.1 (Ar-C), 127.9 (Pyrazole-C), 119.4 (Pyrazole-C), 21.2 (CH$_3$), 10.1 (CH$_3$), 9.3 (CH$_3$). **IR;** (KBr, cm^{-1}): 3117 (sp^{2}CH), 2967 (sp^{3}CH), 1675 (C=O), 1565 (C=N), 1595-1480 (C=C), 601–735 (C-Cl); **GC-MS;** (EI, 70 eV): m/z (%):250 M + 2, 249 M + 1; 248 (M$^+$, ^{37}Cl, 18), 246 (M$^+$, ^{35}Cl, 65), 135 (14), 119 (100), 130 (8), 91 (60), 82 (51); Elemental Analysis: calculated, C, 62.78; H, 5.27; N, 11.26; Found; C, 62.75; H, 5.24; N, 11.22 accurate mass: 248.1.

4.1.1.10. (4-Chloro-3,5-dimethyl-1H-pyrazol-1-yl) (pyridin-4-yl) methanone (3j). Light brown Solid (500 mg, 50%), m. p; 215 °C, R_f; 0.40 (Pet Ether: Ethyl Acetate; 8:2), **¹H NMR;** (300 MHz, CDCl$_3$):

$\delta = 8.79$–7.79 (m, 4H, pyridine), 2.77 (s, 3H, CH$_3$), 2.10 (s, 3H, CH$_3$), **^{13}C NMR;** (75 MHz, CDCl$_3$): $\delta = 166.3$ (C=O), 151.4 (Ar-C), 150.4 (Ar-C), 140.5 (Ar-C), 134.0 (Ar-C), 124.7 (Ar-C), 124.7 (Pyrazole-C), 119.4 (Pyrazol-C), 10.8 (CH$_3$), 9.9 (CH$_3$). **IR;** (KBr, cm^{-1}): 3147 (sp^{2}CH), 2933 (sp^{3}CH), 1673 (C=O), 1560 (C=N), 1597-1489 (C=C), 695-570 (C-Cl); **GC-MS;** (EI, 70 eV): m/z (%):237 M + 2, 236 M + 1; 237 (M$^+$, ^{37}Cl, 19), 235 (M$^+$, ^{35}Cl, 55), 130 (8), 122 (13), 106 (100), 82 (51); Elemental Analysis: calculated C, 56.06; H, 4.28; C N, 17.83; Found C, 56.04; H, 4.27; N, 17.81 accurate mass: 235.2.

4.1.1.11. (E)-1-(4-Chloro-3,5-dimethyl-1H-pyrazol-1-yl)-3-phenylprop-2-en-1-one (3k). Orange Oil (70%), R$_f$; 0.58 (Pet Ether: Ethyl Acetate; 8:2), **^{1}H NMR;** (300 MHz, CDCl$_3$): $\delta = 7.68$ (d, $J = 15.2$ Hz, 1H, Ar-H), 7.60–7.50 (m, 2H, Ar-H), 7.50–7.32 (m, 3H, Ar-H), 6.79 (d, $J = 15.2$ Hz, 1H, Ar-H), 6.17 (s, 1H, CH), 2.5 (s, 3H, CH$_3$),2.3 (s, 3H, CH$_3$), **^{13}C NMR;** (75 MHz, CDCl$_3$): $\delta = 160.2$ (C=O), 150.6 (Ar-C), 150.1 (Ar-C), 135.8 (Ar-C), 135.0 (Ar-C), 129.4 (Ar-C), 129.0 (Ar-C), 129.0 (Ar-C), 128.0 (Ar-C), 128.0 (Ar-C), 119.6 (Pyrazole-C), 117.6 (Pyrazole-C), 10.7 (CH$_3$), 9.9 (CH$_3$). **IR;** (KBr,cm^{-1}): 3122 (sp^{2}CH), 2856 (sp^{3}CH), 1677 (C=O), 1583 (C=N), 1555-1478 (C=C), 700-627 (C-Cl). **GC-MS;** (EI, 70 eV): m/z (%): 262 M + 2, 261 M + 1; 262 (M$^+$, ^{37}Cl, 23), 260 (M$^+$, ^{35}Cl, 67), 147 (12), 131 (100), 130 (8); Elemental Analysis: calculated, C, 64.49; H, 5.03; N, 10.74; Found C, 64.47; H, 5.01; N, 10.72; accurate mass: 260.1.

4.1.1.12. (4-Chloro-3,5-dimethyl-1H-pyrazol-1-yl) (p-tolyl)methanone (3l). Yellow Solid (630 mg, 63%), m. p; 122 °C, R$_f$; 0.48 (Pet Ether: Ethyl Acetate; 8:2), **^{1}H NMR;** (300 MHz, CDCl$_3$): $\delta = 7.85$ (d, 2H, $J = 7.5$ Hz, ArH), 7.25 (d, 2H, $J = 7.5$ Hz, ArH), 2.60 (s, 3H, CH$_3$), 2.4 (s, 3H, CH$_3$), 2.24 (s, 3H, CH$_3$), **^{13}C NMR;** (75 MHz, CDCl$_3$): $\delta = 167.7$ (C=O), 149.2 (Ar-C), 143.6 (Ar-C), 140.2 (Ar-C), 131.5 (Ar-C), 129.5 (Ar-C), 128.6 (Pyrazole-C), 114.62 (Pyrazole-C), 21.6 (CH$_3$), 12.27 (CH$_3$), 11.76 (CH$_3$); **IR;** (KBr, cm^{-1}): 3057 (sp^{2}CH), 2922 (sp^{3}CH), 1701 (C=O), 1683 (C=C), 1509 (C=N), **GC-MS;** (EI, 70 eV): m/z (%):250 M + 2, 249 M + 1; 248(M$^+$, ^{37}Cl, 24), 119 (100), 91 (99), 65 (80); Elemental Analysis: calculated, C, 62.78; H, 5.27; N, 11.26; Found; C, 62.75; H, 5.25; N, 11.24 accurate mass: 248.1.

4.1.1.13. (4-Chloro-3,5-dimethyl-1H-pyrazol-1-yl) (naphthalen-2-yl) methanone (3m). Light brown 720 mg, (72%), m. p; 205 °C, R$_f$; 0.57 (Pet Ether: Ethyl Acetate; 8:2), **^{1}H NMR;** (300 MHz, CDCl$_3$): $\delta = \delta$ 8.14 (d, $J = 15.6$ Hz, 2H, Ar-H), 7.86 (d, $J = 16.8$ Hz, 2H, Ar-H), 7.56 (s, 1H, Ar-H), 7.49 (d, $J = 4.7$ Hz, 2H, Ar-H) 2.62 (s, 3H, CH$_3$), 2.29 (s, 3H, CH$_3$), **^{13}C NMR;** (75 MHz, CDCl$_3$): $\delta = 165.7$ (C=O), 150.8 (Ar-C), 137.0 (Ar-C), 134.5 (Ar-C), 134.0 (Ar-C), 134.0 (Ar-C), 130.3 (Ar-C), 129.7 (Ar-C), 128.7 (Ar-C), 128.2 (Ar-C), 127.0 (Ar-C), 126.5 (Ar-C), 125.5 (Pyrazole-C), 119.4 (Pyrazole-C), 12.7 (CH$_3$), 10.9 (CH$_3$). **IR;** (KBr, cm^{-1}): 3134 (sp^{2}CH), 2969 (sp^{3}CH), 1679 (C=O), 1578 (C=N), 1602-1483 (C=C), 595−725 (C-Cl); **GC-MS;** (EI, 70 eV): m/z (%):286 M + 2, 285 M + 1; 286 (M$^+$, ^{37}Cl, 22), 284 (M$^+$, ^{35}Cl, 70), 171 (12), 155 (100), 130 (9); Elemental Analysis: calculated; C, 67.49; H, 4.60; N, 9.84; Found C, 67.47; H, 4.58; N, 9.81 accurate mass: 284.3.

4.1.1.14. (4-Chloro-3,5-dimethyl-1H-pyrazol-1-yl) (o-tolyl)methanone (3n). Yellow Oil (59%), R$_f$; 0.45 (Pet Ether: Ethyl Acetate; 8:2), **^{1}H NMR;** (300 MHz, CDCl$_3$): $\delta = 7.67$–7.61 (m, 1H, Ar-H), 7.45 (td, $J = 7.5$, 1.5 Hz, 1H, Ar-H), 7.36–7.27 (m, 2H, Ar-H); 2.5 (s, 3H, Pyrazole CH$_3$), 2.4 (s, 3H, Toluene CH$_3$), 2.37 (s, 3H, Pyrazole CH$_3$), **^{13}C NMR;** (75 MHz, CDCl$_3$): $\delta = 163.6$ (C=O), 151.4 (Ar-C), 137.8 (Ar-C), 134.0 (Ar-C), 133.6 (Ar-C), 132.3 (Ar-C), 130.8 (Ar-C), 130.1 (Ar-C), 126.7 (Ar-C), 119.4 (Ar-C), 20.2 (CH$_3$), 10.7 (CH$_3$), 9.9 (CH$_3$); **IR;** (KBr, cm^{-1}): 3140 (sp^{2}CH), 2995 (sp^{3}CH), 1662 (C=O), 1552 (C=N), 1595-1485 (C=C), 605−745 (C-Cl); 1567-1488 (C=C), 1070 (C-O). **GC-MS;** (EI, 70 eV): m/z (%):250 M + 2, 249 M + 1, 248(M$^+$, ^{37}Cl, 22), 246 (M$^+$, ^{35}Cl, 74), 135 (14), 119 (100), 130 (8), 91 (60), 82 (51). Elemental

Analysis: Calculated, C, 62.78; H, 5.27; N, 11.26; Found C, 62.75; H, 5.24; N, 11.23 accurate mass: 248.3.

4.1.1.15. (R)-1-(4-chloro-3,5-dimethyl-1H-pyrazol-1-yl)-2-(4-isobutylphenyl)propan-1-one (3o). Orange Oil (59%), R$_f$; 0.48 (Pet Ether: Ethyl Acetate; 8:2), **^{1}H NMR;** (300 MHz, CDCl$_3$): $\delta = 7.85$ (d, 2H, $J = 7.5$ Hz, ArH), 7.25 (d, 2H, $J = 7.5$ Hz, ArH), 4.64 (1H, q, J 6.99 Hz, CHCH$_3$), 2.41 (3H, d, J 7.10 Hz,CHC<u>H</u>$_3$), 2.40 (s, 3H, CH$_3$), 2.47 (s, 3H, CH$_3$), 1.72 {1.85 (1H, m, CH(CH$_3$)$_2$), 1.39 (3H, d, CHCH$_3$), 0.85 (6H, d, J 6.60 Hz, CH(C<u>H</u>$_3$)$_2$), **^{13}C NMR;** (75 MHz, CDCl$_3$): $\delta = 198.6$ (C=O), 146.4 (Ar-C), 139.83 (Ar-C), 137.8 (Ar-C), 133.6 (Ar-C), 130.8 (Ar-C), 130.11 (Ar-C), 109.5 (Ar-C), 45.24 (CH$_2$), 39.78 (CH), 29.78 (CH$_3$), 22.78 (CH$_3$), 17.78 (CH$_3$), 10.78 (CH$_3$), 8.78 (CH$_3$), **IR;** (KBr, cm^{-1}): 3140 (sp^{2}CH), 2995 (sp^{3}CH), 1662 (C=O), 1552 (C=N), 1595-1485 (C=C), 605−745 (C-Cl); **GC-MS;** (EI, 70 eV): m/z (%):320 M + 2, 319 M + 1; 318(M$^+$, ^{37}Cl, 22), 316 (M$^+$, ^{35}Cl, 74), 161 (14), 157 (100), 129 (8), 91 (60), 189 (51); Elemental Analysis: calculated, C, 67.81; H, 7.27; N, 8.79; Found C, 67.79; H, 7.24; N, 8.76 accurate mass: 318.2.

4.1.1.16. 3,5-Dimethyl-4-(naphthalen-2-yloxy)-1H-pyrazole (4a). Starting with 3-(naphthalen-2-yloxy)pentane-2,4-dione (478 mg, 2.0 mmol) and hydrazine hydrate (100 mg, 2.0 mmol), **4a** was isolated as a pink solid (700 mg, 70%), mp.120 °C; **^{1}HNMR;** (300 MHz, CDCl$_3$): $\delta = 9.32$ (s, 1H, NH), 7.84–7.81 (m, 2H, Ar-H), 7.69 (qd, $J = 7.5$, 1.4 Hz, 2H, Ar-H), 7.46–7.43 (m, 3H, Ar-H), 2.23 (d, $J = 11.5$ Hz, 6H); **^{13}CNMR** (75 MHz, CDCl$_3$): $\delta = 156.5$ (Ar-C), 136.1 (Ar-C), 134.2 (Ar-C), 129.8 (Ar-C), 129.6 (Ar-C), 127.7 (Ar-C), 126.9 (Ar-C), 126.6 (Ar-C), 124.2 (Ar-C), 117.6 (Ar-C), 108.9 (Pyrazole-C), 108.6 (Pyrazole-C), 106.2 (C-O), 19.6 (CH$_3$); **IR;** (KBr, cm^{-1}): 3159 (sp^{2}CH), 2917 (sp^{3}CH), 1629 (C=N), 1597-1508(C=C), 1053(C-O); **GC-MS;** (EI, 70 eV): m/z (%):239 M + 1; 238 (M+, 100), 209 (10), 155 (15), 127 (30), 115 (11), 77 (10); Elemental Analysis: calculated C, 75.61; H, 5.92; N, 11.76 Found C, 75.59; H, 5.89; N, 11.73 accurate mass: 238.1.

4.1.1.17. (4-Aminophenyl) (3,5-dimethyl-4-(p-tolyloxy)-1H-pyrazol-1-yl)methanone (4b). Starting with 3-(p-tolyloxy)pentane-2,4-dione (412 mg, 2.0 mmol) and 4-aminobenzohydrazide (312 mg, 2.0 mmol), **4b** was isolated as a red solid (300 mg, 30%). mp.160 °C; **^{1}HNMR;** (300 MHz, CDCl$_3$): $\delta = 7.57$ (d, $J = 7.5$ Hz, 2H, ArH), 6.97 (d, $J = 7.5$ Hz, 2H, ArH), 6.76–6.67 (m, 4H), 3.82 (s, 2H, NH$_2$), 2.52 (s, 1H, CH$_3$), 2.43 (s, 3H, CH$_3$), 2.32 (s, 3H, CH$_3$), **^{13}CNMR;** (75 MHz, CDCl$_3$): $\delta = 166.3$ (C=O), 153.7 (Ar-C), 152.7 (Ar-C), 141.9 (Ar-C), 140.6 (Ar-C), 134.2 (Ar-C), 131.8 (Ar-C), 131.2 (Ar-C), 128.6 (Ar-C), 128.6 (Ar-C), 125.0 (Ar-C), 122.8 (Ar-C), 119.9 (Ar-C), 117.4 (Ar-C), 112.3 (Pyrazole-C), 110.5 (Pyrazole-C), 21.1 (CH$_3$), 19.5 (CH$_3$), 18.3 (CH$_3$) **IR;** (KBr, cm^{-1}): 3127(sp^{2}CH), 2952(sp^{3}CH), 1670 (C=O), 1573(C=N), 1592-1498(C=C), 1060(C-O); **GC-MS** (EI, 70 eV): m/z (%):322 M + 1; 321 (M+, 100), 209 (7), 119 (35), 91(30), 65 (25), 51 (10); Elemental Analysis: C, 71.01; H, 5.96; N, 13.08 Found C, 71.68; H, 5.94; N, 13.05 accurate mass: 321.1.

4.1.1.18. (4-Chlorophenyl) (3,5-dimethyl-4-(p-tolyloxy)-1H-pyrazol-1-yl)methanone (4c). Starting with 3-(p-tolyloxy)pentane-2,4-dione (412 mg, 2.0 mmol) and 4-chlorobenzo-hydrazide (140 mg, 2.0 mmol), 4c was isolated as a yellow solid.(300 mg, 30%), m. p; 155 °C; **^{1}HNMR;** (300 MHz, CDCl$_3$): $\delta = 7.71$ (d, $J = 7.5$ Hz, 2H, ArH), 7.44 (d, $J = 7.5$ Hz, 2H, ArH), 6.97 (d, $J = 7.5$ Hz, 2H, ArH), 6.72 (d, $J = 7.5$ Hz, 2H, ArH), 2.52 (s, 1H, CH$_3$), 2.42 (s, 1H, CH$_3$), 2.32 (s, 3H, CH$_3$), **^{13}CNMR;** (75 MHz, CDCl$_3$): $\delta = 166.3$ (C=O), 153.7 (Ar-C), 141.9 (Ar-C), 140.6 (Ar-C), 139.7 (Ar-C), 134.1 (Ar-C), 132.8 (Ar-C), 129.8 (Ar-C), 129.8 (Ar-C), 129.2 (Ar-C), 128.8 (Ar-C), 128.6 (Ar-C), 127.9 (Ar-C), 125.0 (Ar-C), 119.9 (Pyrazole-C), 117.1 (Pyrazole-C), 21.1 (CH$_3$), 18.3 (CH$_3$), 17.6 (CH$_3$) **IR;** (KBr, cm^{-1}): 3095 (sp^{2}CH), 2919

(sp^{3}CH), 1640 (C=O); 1586 (C=N), **GC-MS** (EI, 70 eV): *m/z* (%):342 M + 2, 341 M + 1; 340 (M$^+$,^{37}Cl, 24), 238 (M$^+$,^{35}Cl, 54), 207 (26), 164 (16), 139 (100), 111 (44), 91 (15); Elemental Analysis: calculated C, 66.96; H, 5.03; N, 8.22; Found C, 66.93; H, 5.01; N, 8.20 accurate mass: 340.1.

*4.1.1.19. 1-(4-aminobenzoyl)-5-methyl-1H-pyrazol-3(2H)-one (**5a**).* Starting with ethyl 3-oxobutanoate (200 mg, 2.0 mmol), 4-amino benzohydrazide (302 mg, 2.0 mmol), and added a drop of concentrated sulphuric acid. **5a** was isolated as a pink Solid (714 mg, 72%), m. p; 158 °C, R$_f$; 0.62 (Pet Ether: Ethyl Acetate; 8:2), **^{1}HNMR;** (300 MHz, CDCl$_3$): δ = 10.24 (s, 1H, NH), 7.95 (d, 2H, *J* = 8.0 Hz, ArH), 6.58 (d, 2H, *J* = 7.5 Hz, ArH), 6.07 (s, 1H, CH), 2.6 (s, 3H, CH$_3$), 2.29 (s, 3H, CH$_3$), 4.10 (s, 2H, NH$_2$); **^{13}C NMR;** (75 MHz, CDCl$_3$): δ = 192.5 (C=O), 166.7 (C=O), 152.7 (Ar-C), 138.7 (Ar-C), 131.8 (Ar-C), 130.5 (Ar-C), 122.8 (Ar-C), 113.4 (Ar-C), 112.3 (Pyrazole-C), 110.5 (Pyrazole-C), 13.67 (CH$_3$), 10.8 (CH$_3$). **IR;** (KBr, cm^{-1}): 3131 (sp^{2}CH), 2923 (sp^{3}CH), 1513 (C=N), 1661 (C=O), 1597-1479 (C=C), 3437 (NH); **GC-MS;** (EI, 70 eV): *m/z* (%):218 M + 1; 217(10), 97(12), 120 (100), 92 (60); Elemental Analysis: calculated, C, 60.82; H, 5.10; N, 19.34; Found; C, 60.80; H, 5.08; N, 19.31 accurate mass: 217.1.

*4.1.1.20. 3-methyl-2-(4-methylbenzoyl)-1,2-dihydropyrazol-5-one (**5b**).* Starting with ethyl 3-oxobutanoate (204 mg, 2.0 mmol), 4-methyl benzohydrazide (301 mg, 2.0 mmol), and added a drop of concentrated sulphuric acid. **5b** was isolated as a pink Solid (714 mg, 72%), m. p; 158 °C, R$_f$; 0.62 (Pet Ether: Ethyl Acetate; 8:2), **^{1}HNMR;** (300 MHz, CDCl$_3$): δ = 10.21 (s, 1H, NH), 7.85 (d, 2H, *J* = 8.0 Hz, ArH), 6.78 (d, 2H, *J* = 7.5 Hz, ArH), 6.06 (s, 1H, CH), 2.71 (s, 3H, CH$_3$), 2.39 (s, 3H, CH$_3$), 4.12 (s, 2H, NH$_2$); **^{13}C NMR;** (75 MHz, CDCl$_3$): δ = 182.57 (C=O), 167.7 (C=O), 151.71 (Ar-C), 138.73 (Ar-C), 131.71 (Ar-C), 131.61 (Ar-C), 122.77 (Ar-C), 113.49 (Ar-C), 112.34 (Pyrazole-C), 112.34 (Pyrazole-C), 12.67 (CH$_3$), 10.19 (CH$_3$); **IR;** (KBr, cm^{-1}): 3131(sp^{2}CH), 2923(sp^{3}CH), 1513(C=N), 1661(C=O), 1597-1479(C=C), 3437(NH); **GC-MS;** (EI, 70 eV): *m/z* (%): 217 M + 1; 216(10), 97(12), 109 (100), 91 (60); Elemental Analysis: calculated C, 66.65; H, 5.59; N, 12.96; Found C, 66.61; H, 5.55; N, 12.93, accurate mass: 216.1.

4.2. Biological protocols

4.2.1. Cell transfection and preparation of membrane fractions

Initially, the plasmids expressing alkaline phosphatase (*h*-TNAP & *h*-IAP) [41] or human nucleotide pyrophosphatase/phosphodiesterase (*h*-NPP1 & *h*-NPP3) [42,43] were transfected into the COS-7 cells, using lipofectamine. Next day, serum free dulbecco's modified eagle's medium (DMEM); containing plasmid DNA (6 µg) and lipofectamine reagent (24 µL) was added to the transfected cells and the plates were kept under incubation at 37 °C for 5 h. After 48 h, the transfection reaction was stopped by replacing the serum free media with the media containing 20% FBS. After incubation of 48—72 h, the transfected cells were washed with tris-saline buffer and further processed as reported earlier [44]. For the transfection of NTPDases, chinese hamster ovary (CHO) cells were transfected by using electroporation method as described previously [45]. Briefly, CHO cells were transfected with plasmid expressing rat NTPDase1 [46] or NTPDase2 [47] or rat NTPDase3 [45] by using a BTX Electrocell manipulator 600. NTPDase was transfected and purified by previously used protocol [39]. The total protein estimation was carried out by Bradford method and the aliquotes of protein were kept at −80 °C after the addition of 7.5% glycerol [48].

4.2.2. Alkaline phosphatase inhibition assay (h-TNAP & h-IAP)

The alkaline phosphatase (*h*-TNAP and *h*-IAP) inhibition assay

was carried out as discussed in our previously published article [49]. For the inhibition assay, 10 µL of each tested compound was pre-treated with 20 µL of *h*-TNAP (46 ng/well) or *h*-IAP (57 ng/well) isozyme. The reaction mixture was kept at 37 °C for 5—10 min and luminescence signals were recorded by using FLx800 microplate reader (BioTek ™, Instruments, Inc. USA). Finally, 20 µL of CDP-star$^®$ substrate was added to each reaction well and after 20 min of incubation, the signals were again measured. The data was analyzed by using PRISM 5.0 (GraphPad, San Diego, California, USA) software and the inhibitory concentration values (IC$_{50}$ values) of the most effective derivatives were determined as discussed earlier [49].

4.2.3. Nucleotide pyrophosphatase/phosphodiesterase (h-NPP1 & h-NPP3) inhibition assay

The nucleotide pyrophosphatase (*h*-NPP1 & *h*-NPP3) inhibitory assay was performed as reported earlier [50]. Intially, to the each well, 10 µL of tested compound, 10 µL of *h*-NPP1 (final conc. of 27 ng) or *h*-NPP3 (final conc. of 25 ng) and 70 µL of 50 mM tris- HCl (pH 9.5) buffer were added and kept at 37 °C for 5—10 min. After incubation, absorbance was determined at 405 nm using ELx800 microplate reader (BioTek,™ Instruments, Inc. USA). Finally, 10 µL of substrate *p*-nitrophenyl-5′-thymidine monophosphate (*p*-Nph-5′-TMP, 0.5 mM) was added to each reaction mixture and change in absorbance was evaluated after 35 min of incubation. The PRISM 5.0 (GraphPad, San Diego, California, USA) software was used for data analysis and the inhibitory concentration values (IC$_{50}$ values) were determined as mentioned in previous publication [50].

4.2.4. Nucleoside triphosphate diphosphohydrolase (r-NTPDase1, 2, 3 & 8) inhibition assay

All the synthesized derivatives were tested for their *r*-NTPDase activity by slightly modifying the previously reported method [51]. The assay buffer containing 50 mM tis-HCl supplemented with 5 mM CaCl$_2$ (pH 7.4) was used. The total assay volume of 100 µL contained 59 µL of assay buffer, 10 µL of tested compound and 6 µL of *r*-NTPDase1 (final conc. of 0.99 µg) or *r*-NTPDase2 (final conc. of 1.21 µg) or *r*-NTPdase3 (final conc. of 1.04 µg) or *r*-NTPdase8 (final conc. of 1.85 µg). The reaction mixture was allowed to incubate at 37 °C for 10 min and absorbance was measured at 630 nm using microplate reader (BioTek ELx800, Instruments, Inc. USA). Reaction was initiated by the addition of 10 µL of adenosine triphosphate (0.5 mM) and the reaction mixture was again incubated at 37 °C for 10 min followed by the addition of 15 µL of malachite green reagent. The change in absorbance was measured within 3—5 min of incubation. The compounds having more than 50% inhibition of any isoform of *r*-NTPDase were further evaluated to determine the IC$_{50}$ values. The IC$_{50}$ values were determined by using non-linear curve fitting program PRISM 5.0 (GraphPad, San Diego, California, USA).

4.2.5. Molecular docking methodology

The molecular docking studies of the most effective inhibitors i.e., **3g**, **3a**, **4c** and **3l** were performed to find out the most possible binding interactions of the identified effective derivatives within the selected targeted enzymes i.e., *h*-TNAP, *h*-IAP, *h*-NPP1 and *h*-NPP3, respectively. The x-ray crystallographic structures of *h*-TNAP, *h*-IAP, *h*-NPP1 and *h*-NPP3 are not reported in Protein Data Bank (PDB) till to-date so already published homology models from our research groups were used for docking studies [52,53]. Prior to the docking studies, the homology models were refined and protonated using AMBER99 force field and energy was minimized with a RMSD gradient of <0.05 kcal/mol/Å using Molecular Operating Environment (MOE, 2014.09) [54]. The structures of all effective inhibitors were generated using the builder tool within MOE software. Then hydrogen atoms were added to all compounds and charges were assigned to each atom. Finally the energy

minimization of compounds structure was carried using force field MMFF94x with RMSD gradient of <0.01 kcal/mol/Å. After preparation of protein structures and compounds, MOE Site finder utility was used to identify the binding sites within all target enzymes. MOE Site finder uses a geometric approach to find the possible binding sites in a protein structure starting from its 3D atomic coordinates. For docking calculation default triangle matcher placement method and default scoring function GBVI/WSA ΔG were used which estimates free binding energy of bound ligand within active site. After completion of docking calculation, those possess which were with the lowest S score and free binding energies were selected further for visualizing the putative binding interactions within the active site of all selected enzymes. Discovery studio 4.0 and PoseView BioSolveIT GmbH, Germany were used for 3D and 2D visualization purpose, respectively [55,56].

4.2.6. Cell viability assays (MTT assay)

The cytotoxic potential of the synthesized pyrazole derivatives was scrutinized against three different cancer cell lines i.e., breast cancer cells (MCF-7), cervical cancer cells (HeLa) and bone marrow cells i.e., Lymphoblast cells (k-562). The assay was performed by using MTT (Dimethyl–2–thiazolyl–2,5–diphenyl–2H–tetrazolium bromide)–based cell viability assay [57] and [58] as discussed earlier [59].

Acknowledgement

Appendix A. Supplementary data

Supplementary data related to this article can be found at https://doi.org/10.1016/j.ejmech.2018.07.002.

References

[1] L.N. Johnson, R.J. Lewis, Structural basis for control by phosphorylation, Chem. Rev. 101 (2001) 2209–2242.
[2] J.A. Adams, Kinetic and catalytic mechanisms of protein kinases, Chem. Rev. 101 (2001) 2271–2290.
[3] J. Krol, I. Loedige, W. Filipowicz, The widespread regulation of microRNA biogenesis, function and decay, Nat. Rev. Genet. 11 (2010) 597–610.
[4] S.M. Keyse, Protein phosphatases and the regulation of mitogen-activated protein kinase signalling, Curr. Opin. Cell Biol. 12 (2000) 186–192.
[5] P. Romero, J. Wagg, M.L. Green, D. Kaiser, M. Krummenacker, P.D. Karp, Computational prediction of human metabolic pathways from the complete human genome, Genome Biol. 6 (2005). R2–R2.
[6] C. Munoz-Pinedo, J.E. Ricci, N. El Mjiyad, Cancer metabolism: current perspectives and future directions, Cell Death & Disease. 3 (1) (2012) e248.
[7] H. Guanhua, Q. Cui, QM/MM analysis suggests that alkaline phosphatase (AP) and nucleotide pyrophosphatase/phosphodiesterase slightly tighten the transition state for phosphate diester hydrolysis relative to solution: implication for catalytic promiscuity in the AP superfamily, J. Am. Chem. Soc. 134 (2011) 229–246.
[8] M.F. Hoylaerts, L. Ding, S. Narisawa, S. Van Kerckhoven, J.L. Millán, Mammalian alkaline phosphatase catalysis requires active site structure stabilization via the N-terminal amino acid microenvironment, Biochemist 45 (2006) 9756–9766.
[9] S. Jangra, N. Raghav, Inhibitors of alkaline phosphatase: a review, Nat. J. Basic. App. Sci. 1 (2012) 91–97.
[10] M. Hui, M. Hu, H.C. Tenenbaum, Changes in cell adhesion and cell proliferation are associated with expression of tissue non-specific alkaline phosphatase, Cell Tissue Res. 274 (1993) 429–437.
[11] E.G. Giannini, R. Testa, V. Savarino, Liver enzyme alteration: a guide for clinicians, CMAJ (Can. Med. Assoc. J.) 172 (2005) 367–379.
[12] R.E. Coleman, Clinical features of metastatic bone disease and risk of skeletal morbidity, Clin. Canc. Res. 12 (2006) 6243s–6249s.
[13] M.J. Blayney, R.L. Pisoni, J.L. Bragg-Gresham, J. Bommer, L. Piera, A. Saito, T. Akiba, M.L. Keen, E.W. Young, F.K. Port, High alkaline phosphatase levels in hemodialysis patients are associated with higher risk of hospitalization and

[14] C. Stefan, S. Jansen, M. Bollen, NPP-type ectophosphodiesterases: unity in diversity, Trends Biochem. Sci. 30 (2005) 542–550.
[15] J. Stella, L. Bavaresco, E. Braganhol, L. Rockenbach, P.F. Farias, M.R. Wink, A.A. Azambuja, C.H. Barrios, F.B. Morrone, A.M.O. Battastini, Differential ectonucleotidase expression in human bladder cancer cell lines, Urol. Oncol. Seminars and Original Invest 28 (2010) 260–267.
[16] M. al-Rashida, J. Iqbal, Therapeutic potentials of ecto-nucleoside triphosphate diphosphohydrolase, ecto-nucleotide pyrophosphatase/phosphodiesterase, ecto-5′-nucleotidase, and alkaline phosphatase inhibitors, Med. Res. Rev. 34 (2014) 703–743.
[17] J. Lecka, G. Ben-David, L. Simhaev, S. Eliahu, J. Oscar Jr., P. Luyindula, J. Pelletier, B. Fischer, H. Senderowitz, J. Sévigny, Nonhydrolyzable ATP analogues as selective inhibitors of human NPP1: a combined computational/ experimental study, J. Med. Chem. 56 (2013) 8308–8320.
[18] J.W. Goding, B. Grobben, H. Slegers, Physiological and pathophysiological functions of the ecto-nucleotide pyrophosphatase/phosphodiesterase family, Biochim. Biophys. Acta (BBA) - Mol. Basis Dis. 1638 (2003) 1–19.
[19] A. Gartland, I.R. Orriss, R.M. Rumney, A.P. Bond, T. Arnett, J.A. Gallagher, Purinergic signalling in osteoblasts, Front. Biosci. 17 (2012) 16–29.
[20] S. Mebarek, E. Hamade, C. Thouverey, J. Bandorowicz-Pikula, S. Pikula, D. Magne, R. Buchet, Ankylosing spondylitis, late osteoarthritis, vascular calcification, chondrocalcinosis and pseudo gout: toward a possible drug therapy, Curr. Med. Chem. 18 (2011) 2196–2203.
[21] J.L. Millán, The role of phosphatases in the initiation of skeletal mineralization, Calcif. Tissue Int. 93 (2013) 299–306.
[22] F.M. Sansom, The role of the NTPDase enzyme family in parasites: what do we know, and where to from here, Parasitology 139 (2012) 963–980.
[23] J. Stella, L. Bavaresco, E. Braganhol, L. Rockenbach, P.F. Farias, M.R. Wink, A.A. Azambuja, C.H. Barrios, F.B. Morrone, A.M.O. Battastini, Differential ectonucleotidase expression in human bladder cancer cell lines, in: Urologic Oncology: Seminars and Original Investigations, 28, Elsevier, 2010 May, pp. 260–267.
[24] E.E. Golub, K. Boesze-Battaglia, The role of alkaline phosphatase in mineralization, Curr Orthop Pract 18 (2007) 444–448.
[25] M. al-Rashida, S.A. Ejaz, S. Ali, A. Shaukat, M. Hamayoun, M. Ahmed, J. Iqbal, Diarylsulfonamides and their bioisosteres as dual inhibitors of alkaline phosphatase and carbonic anhydrase: structure activity relationship and molecular modelling studies, Bioorg. Med. Chem. 23 (2015) 2435–2444.
[26] T.N. Ngo, S.A. Ejaz, T.Q. Hung, T.T. Dang, J. Iqbal, J. Lecka, J. Sévigny, P. Langer, Efficient one-pot synthesis of 5-perfluoroalkylpyrazoles by cyclization of hydrazone dianions, Org. Biomol. Chem. 13 (2015) 8277–8290.
[27] S. Narisawa, D. Harmey, M.C. Yadav, W.C. O'Neill, M.F. Hoylaerts, J.L. Millán, Novel inhibitors of alkaline phosphatase suppress vascular smooth muscle cell calcification, J. Bone Miner. Res. 22 (2007) 1700–1710.
[28] M. al-Rashida, R. Raza, G. Abbas, M.S. Shah, G.E. Kostakis, J. Lecka, J. Sévigny, M. Muddassar, C. Papatriantafyllopoulou, J. Iqbal, Identification of novel chromone based sulfonamides as highly potent and selective inhibitors of alkaline phosphatases, Eur. J. Med. Chem. 66 (2013) 438–449.
[29] P.C. Lv, H.Q. Li, J. Sun, Y. Zhou, H.L. Zhu, Synthesis and biological evaluation of pyrazole derivatives containing thiourea skeleton as anticancer agents, Bioorg. Med. Chem. 18 (2010) 4606–4614.
[30] A.A. Bekhit, T. Abdel-Aziem, Design, synthesis and biological evaluation of some pyrazole derivatives as anti-inflammatory-antimicrobial agents, Bioorg. Med. Chem. 2004 (12) (2004) 1935–1945.
[31] A. Saeed, F.A. Larik, P.A. Channar, Recent synthetic approaches to fipronil, a super-effective and safe pesticide, Res. Chem. Intermed. 42 (2016) 1–9.
[32] O.I. El-Sabbagh, M.M. Baraka, S.M. Ibrahim, C. Pannecouque, G. Andrei, R. Snoeck, J. Balzarini, A.A. Rashad, Synthesis and antiviral activity of new pyrazole and thiazole derivatives, Eur. J. Med. Chem. 44 (2009) 3746–3753.
[33] G.K. Gupta, A. Kumar, 3D-QSAR studies of some tetrasubstituted pyrazoles as COX-II inhibitors, Acta Pol. Pharm. 69 (2012) 763–772.
[34] H. Kiyani, F. Albooyeh, S. Fallahnezhad, Synthesis of new pyrazolyl-1,3-diazabicyclo[3.1.0]hexe-3-ene derivatives, J. Mol. Struct. 1091 (2015) 163–169.
[35] A. Ansari, A. Ali, M. Asif, Biologically active pyrazole derivatives, New J. Chem. 41 (2017) 16–41.
[36] A.A. Saeed, F. Larik, P.A. Channar, Synthetic approaches to the multifunctional drug ebselen and analogs: past and present, Mini-Reviews Org. Chem. 13 (2016) 312–324.
[37] A. Saeed, U. Shaheen, A. Hameed, F. Kazmi, Synthesis and antimicrobial activity of some novel 2-(substituted fluorobenzoylimino)-3-(substituted fluorophenyl)-4-methyl-1, 3-thiazolines, J. Fluorine Chem. 131 (2010) 333–339.
[38] M. Sher, P. Ali, Z. Ashraf, M. Aamir, E. Ahmed, A. Sharif, N. Riaz, S. Iqbal, Synthesis and characterization of some novel 4-aryloxy substituted pyrazoles, Asian J. Chem. 26 (2014) 743–745.
[39] M. al-Rashida, G. Batool, A. Sattar, S.A. Ejaz, S. Khan, J. Lecka, J. Sévigny, A. Hameed, J. Iqbal, 2-Alkoxy-3-(sulfonylarylaminomethylene)-chroman-4-ones as potent and selective inhibitors of ectonucleotidases, Eur. J. Med. Chem. 115 (2016) 484–494.
[40] T.T. Talele, S.A. Khedkar, A.C. Rigby, Successful applications of computer aided drug discovery: moving drugs from concept to the clinic, Curr. Top. Med. Chem. 10 (2010) 127–141.
[41] F. Kukulski, S.A. Lévesque, E.G. Lavoie, J. Lecka, F. Bigonnesse, A.F. Knowles, C.S. Robson, T.L. Kirley, J. Sévigny, Comparative hydrolysis of P2 receptor

agonists by NTPDases 1, 2, 3 and 8, Purinergic Signal. 1 (2005) 193—195.

[42] S.I. Belli, J.W. Goding, Biochemical characterization of human PC-1, an enzyme possessing alkaline phosphodiesterase I and nucleotide pyrophosphatase activities, Eur. J. Biochem. 226 (1994) 433—443.

[43] P. Jinhua, J.W. Goding, H. Nakamura, K. Sano, Molecular cloning and chromosomal localization of PD-Iβ (PDNP3), a new member of the human phosphodiesterase I genes, Genomics 45 (1997) 412—415.

[44] Y. Bravo, P. Teriete, R.P. Dhanya, R. Dahl, P. San Lee, T. Kiffer-Moreira, S. Ganji, R.E. Sergienko, L.H. Smith, C. Farquharson, Design, synthesis and evaluation of benzoisothiazolones as selective inhibitors of PHOSPHO1, Bioorg. Med. Chem. Lett 24 (2014) 4308—4311.

[45] T. Vorhoff, H. Zimmermann, J. Pelletier, J. Sévigny, N. Braun, Cloning and characterization of the ecto-nucleotidase NTPDase3 from rat brain: predicted secondary structure and relation to other members of the E-NTPDase family and actin, Purinergic Signal. 1 (2005) 259—270.

[46] P. Heine, N. Braun, H. Zimmermann, Functional characterization of rat ecto-ATPase and ecto-ATP diphosphohydrolase after heterologous expression in CHO cells, Eur. J. Biochem. 262 (1999) 102—107.

[47] B. Kegel, N. Braun, P. Heine, C.R. Maliszewski, H. Zimmermann, An ecto-ATPase and an ecto-ATP diphosphohydrolase are expressed in rat brain, Neuropharmacology 36 (1997) 1189—1200.

[48] M.M. Bradford, A rapid and sensitive method for the quantitation of microgram quantities of protein utilizing the principle of protein-dye binding.Anal, Biochemist 72 (1976) 248—251.

[49] S.A. Ejaz, A. Saeed, M.N. Siddique, Z. un Nisa, S. Khan, J. Lecka, J. Sévigny, J. Iqbal, Synthesis, characterization and biological evaluation of novel chalcone sulfonamide hybrids as potent intestinal alkaline phosphatase inhibitors, Bioorg. Chem. 70 (2017) 229—236.

[50] E. Ausekle, S.A. Ejaz, S.U. Khan, P. Ehlers, A. Villinger, J. Lecka, J. Sévigny, J. Iqbal, P. Langer, New one-pot synthesis of N-fused isoquinoline derivatives

by palladium-catalyzed C—H arylation: potent inhibitors of nucleotide pyrophosphatase-1 and -3, Org. Biomol. Chem. 14 (2016) 11402—11414.

[51] S.A. Lévesque, E.G. Lavoie, J. Lecka, F. Bigonnesse, J. Sévigny, Specificity of the ecto-ATPase inhibitor ARL 67156 on human and mouse ectonucleotidases, Br. J. Pharmacol. 152 (2007) 141—150.

[52] I. Khan, A. Ibrar, S.A. Ejaz, S.U. Khan, S.J. Shah, S. Hameed, J. Simpson, J. Lecka, J. Sévigny, J. Iqbal, Influence of the diversified structural variations at the imine functionality of 4-bromophenylacetic acid derived hydrazones on alkaline phosphatase inhibition: synthesis and molecular modelling studies, RSC Adv. 5 (2015) 90806—90818.

[53] B. Jafari, N. Yelibayeva, M. Ospanov, S.A. Ejaz, S. Afzal, S.U. Khan, Z.A. Abilov, M.Z. Turmukhanova, S.N. Kalugin, S. Safarov, J. Lecka, Synthesis of 2-arylated thiadiazolopyrimidones by Suzuki—Miyaura cross-coupling: a new class of nucleotide pyrophosphatase (NPPs) inhibitors, RSC Adv. 6 (2016) 107556—107571.

[54] MOE, version 2014.0901, Chemical Computing Group (CCG), Montreal, Canada, http://www.chemcomp.com/MOEMolecular_Operating_Environment.htm.

[55] D.S. Visualizer, Discovery Studio Visualizer, 2, Accelrys Software Inc, 2005.

[56] LeadIT, 2014, at http://www.biosolveit.de/LeadIT/.

[57] T. Mosmann, Rapid colorimetric assay for cellular growth and survival: application to proliferation and cytotoxicity assays, J. Immunol. Meth. 65 (1983) 55—63.

[58] M. Nikš, M. Otto, Towards an optimized MTT assay, J. Immunol. Methods 130 (1990) 149—151.

[59] S. Hassan, S.A. Ejaz, A. Saeed, M. Shehzad, S.U. Khan, J. Lecka, J. Sévigny, G. Shabir, J. Iqbal, 4-Aminopyridine based amide derivatives as dual inhibitors of tissue non-specific alkaline phosphatase and ecto-5'-nucleotidase with potential anticancer activity, Bioorg. Chem. 76 (2017) 237—248.